USGS
science for a changing world

Subsurface Structure and Seismic Velocities As Determined From High-Resolution Seismic Imaging in the Victorville, California area: Implications for Water Resources and Earthquake Hazards

by

R. D. Catchings, B. F. Cox, M. R. Goldman, G. Gandhok, M. J. Rymer, J. Dingler, P. Martin, A. Christensen, and E. Horta

Open-File Report 00-123

2000

U. S. DEPARTMENT OF THE INTERIOR
U.S. GEOLOGICAL SURVEY

Menlo Park, California

Table of Contents

List of Tables

List of Figures

Introduction

Victorville, California is located in the Mojave Desert approximately 130 km northeast of Los Angeles (Fig. 1a). The current population of the Victorville region (including the towns of Adelanto, Apple Valley, Hesperia, and Victorville; locally referred to as the Victor Valley) has increased threefold, from about 90,000 in 1980 to more than 270,000 in 1993 (Victorville Chamber of Commerce, 1994). The large increase in population raises concerns of water-resource availability and of earthquake hazards because of its proximity to the San Andreas and the Garlock fault systems.

The arid climate and growing population put high demands on the groundwater supply, the principal source of water for the region. Groundwater pumping since the late 1800's has resulted in declining water-level and decreases in natural groundwater discharge to the Mojave River, which is the principal source of surface water in the region. The U. S. Geological Survey's Water Resources Division (USGS-WRD) monitors the surface-water flow of the Mojave River near the northern end of the city of Victorville at a constricted area referred to as the Lower Narrows. Another constriction in the river also occurs near the southern end of the city in an area referred to as the Upper Narrows. Although there is surface flow in the Mojave River during a few periods of perennial flow and periods of flow after intense storms, most of the water associated with the Mojave River occurs as groundwater.

The earthquake hazards in the region are of great concern because of the growing population within the Victorville region, the possible effects that earthquakes may have on groundwater flow in the region, and because of the major lifelines (gas, electrical, transportation, etc) that trend through the area to the greater Los Angeles urban corridor. Strong shaking originating from earthquakes on the San Andreas, Garlock, or unmapped faults beneath or near the Victorville region may directly or indirectly affect a wide region of southern California by disrupting the supply of water, gas, and electricity to areas distant from Victorville. Locally, shaking could be amplified by the alluvial sediments beneath the Victorville area. Little is known about seismic velocities, thicknesses, and the subsurface geometry of the alluvial fill; thus, accurate estimates of potential losses to local property and infrastructure, the hazard to the regional water supply, and the hazard to southern California lifelines from earthquakes in the Victorville region cannot be determined at present.

To investigate problems related to both water resources and earthquake hazards in the Victorville area, the U. S. Geological Survey's Geologic Division (USGS-GD) conducted three high-resolution seismic reflection/refraction surveys within the city of Victorville in December 1997 and January of 1998. The seismic surveys were conducted across and within the Mojave River channel at the Upper and Lower Narrows, and southwestward from near the Mojave River to residential areas in the city (Fig. 1b). The surveys were designed to: (1) determine the depth to bedrock across the Mojave River at the Upper and Lower Narrows and to the west of

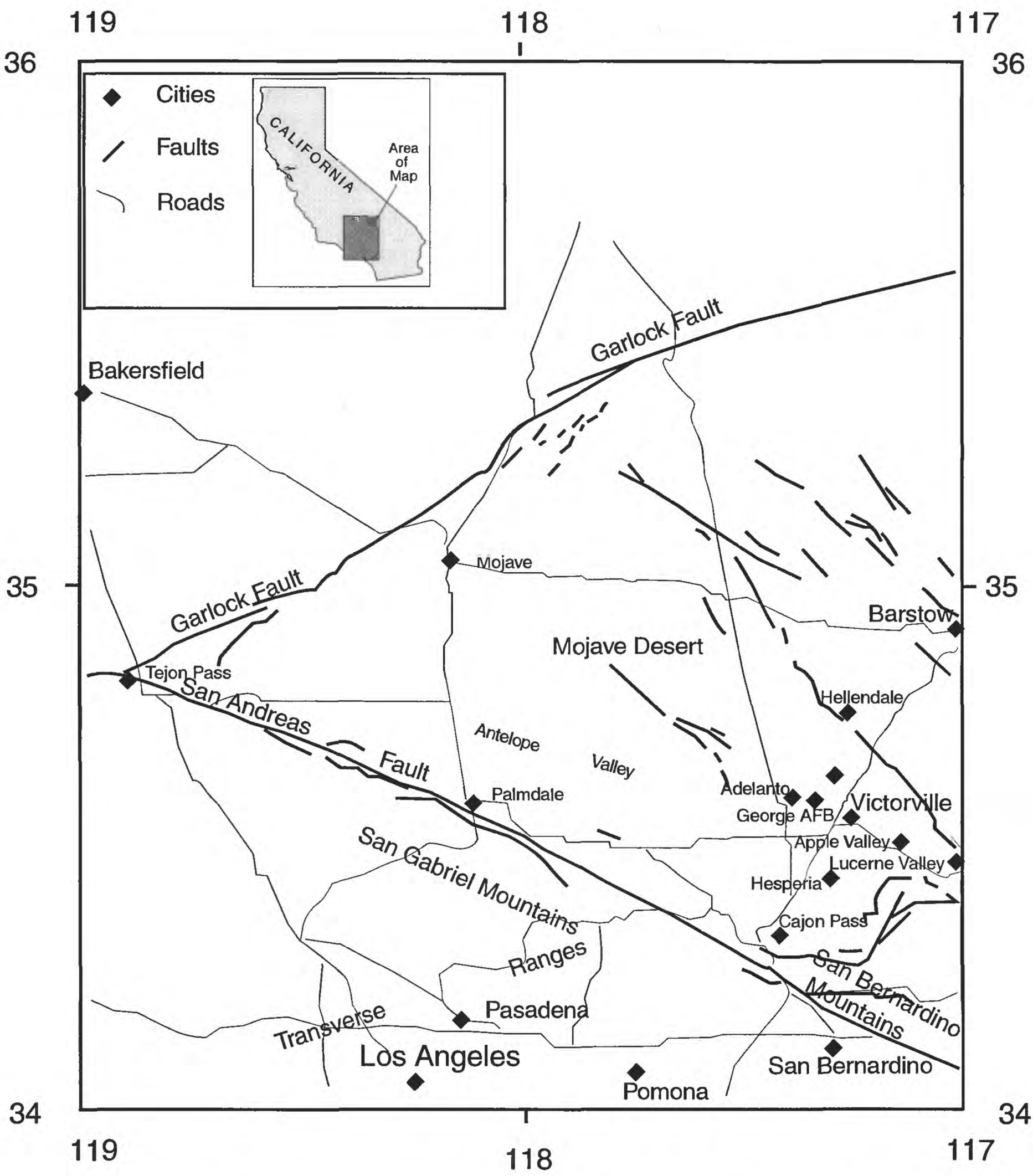

Fig. 1a Regional location of the Victorville, California area with major faults.

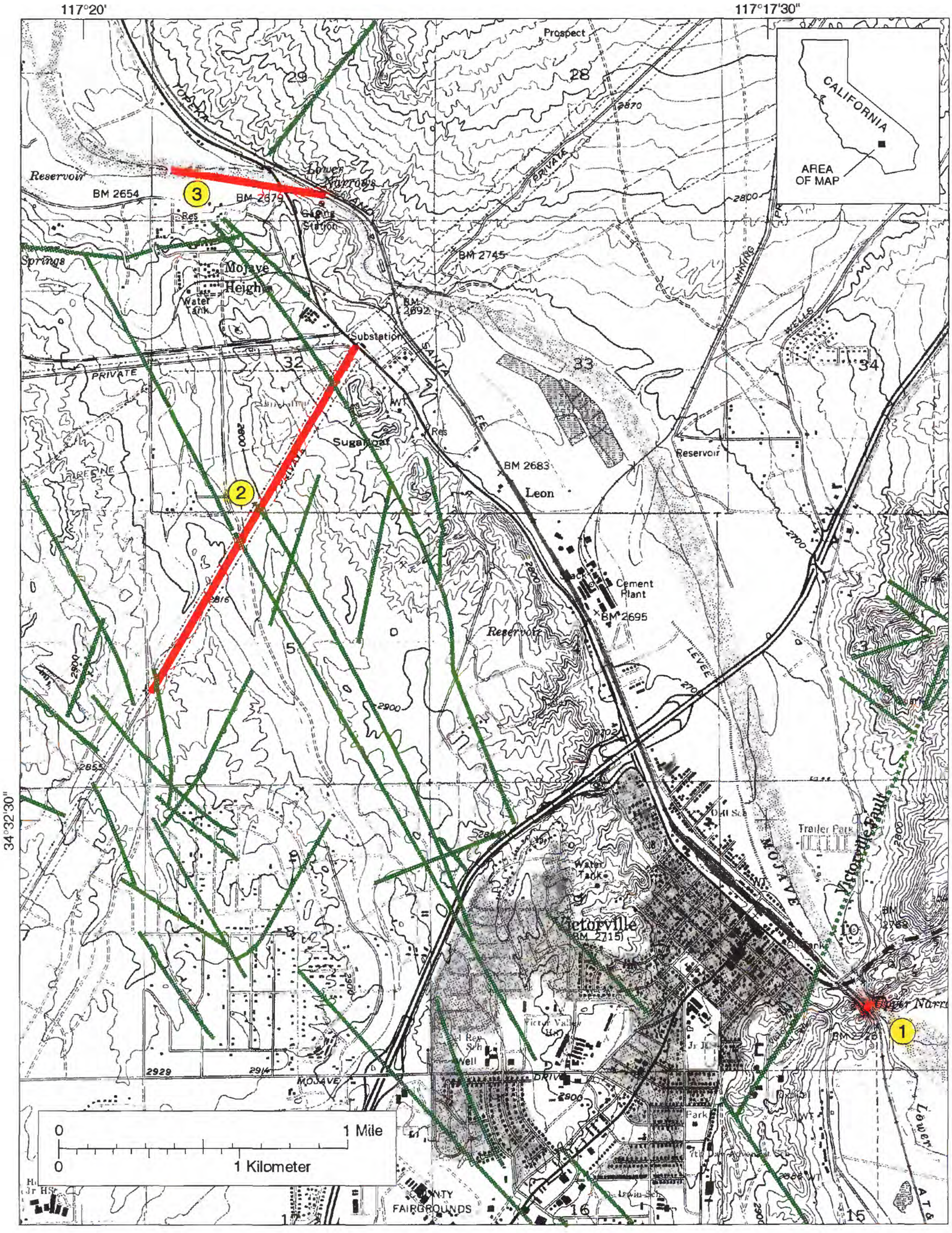

Fig. 1b. Map of Victorville showing location of seismic lines (thick red lines) 1, 2, and 3. Green lines are geologic lineaments (Cox, unpub. map) including Victorville Fault of Bowen (1954); dotted where concealed.

the Mojave River within the city of Victorville, (2) locate possible buried stream channels that may divert groundwater from the Mojave River, (3) locate previously unmapped faults that may affect groundwater flow and that may represent significant seismic hazards, and (4) determine seismic velocities and basin geometries, both of which affect ground shaking during large earthquakes on either regional fault systems (San Andreas and Garlock Faults) or on local unmapped faults.

Geohydrological Setting

The Victor Valley is part of the Mojave River groundwater basin in the Mojave Desert region of southern California. The climate is characterized by low precipitation, low humidity, and high summer temperatures. The Mojave River, which bisects the study area, originates in the foothills of the San Bernardino Mountains and flows northward toward Victorville. In the study area, perennial streamflow occurs only in the mountains and near Victorville, where a basin constriction created by shallow bedrock, locally referred to as the "Narrows", causes groundwater to discharge to the river.

The Mojave River groundwater basin is divided into five subareas: Alto, Baja, Centro, Este, and Oeste. The Alto subarea has a component called the Transition Zone, which is the area between the Lower Narrows and the Centro subarea. Historically, some of the subareas receive at least a portion of their recharge from adjacent upstream subareas, either as surface flow or as groundwater flow.

Geologic Setting

Victorville lies near the northeast margin of a broad alluvial basin in the southern Mojave Desert. Some workers have termed this feature the Cajon basin (e.g., Dibblee, 1967, fig. 71), but we will call it the Victorville basin to avoid confusion with the drainage basin of Cajon Creek, which lies nearby to the south. Isolated ridges and the Mojave River canyon locally border the northeast margin of the Victorville basin. To the south, the basin is framed by the San Gabriel and the San Bernardino Mountains-bold segments of the Transverse Ranges uplifted astride the San Andreas Fault Zone.

Several geologic studies have investigated bodies of pre-Cenozoic rocks that crop out directly north and east of Victorville (Bowen, 1954; Dibblee, 1960, 1967; Miller, 1981). These bodies include two ridges of coarse-grained granitic rocks, consisting mainly of quartz monzonite and granodiorite, that slope southwestward into the Mojave River canyon at the Upper and Lower Narrows (see topography on Fig. 1b). Such granitic rock types are widely distributed in the San Bernardino Mountains and southern and western Mojave Desert (Dibblee, 1967; Bortugno and Spittler, 1986), and similar rocks may form much of the basement floor beneath the Victorville basin. In addition to the granitic rocks, there are also significant Paleozoic metasedimentary rocks (including slate, sandstone, shale, chert, conglomerate, limestone, dolomite, marble, phyllite, schist, hornfels, and quartzite) and Mesozoic volcanic and metavolcanic rocks (including andesite

and rhyolite flow rocks, greenstone, volcanic breccia and other pryoclastic rocks--some of which are strongly metamorphosed, basaltic pillow lava, and diabase), that crop out northwest, north, east, and southeast of the profiles (Jennings, 1977). These rocks, the granitic rocks, or some combination may form the basement rocks beneath much of the Victorville area.

Regional gravity surveys (Mabey, 1960; Subsurface Surveys, 1990; R. Jachens, unpub. data) show that the Victorville basin comprises two sub-basins centered south and west of Victorville, at Hesperia and Adelanto, with maximum depths of about 1.5 km and 1.1 km, respectively. The boundary between the Hesperia and Adelanto sub-basins consists of a subsurface basement ridge projecting southwestward from the Lower Narrows of the Mojave River. Because of this feature, and due to the proximity of the basin margin, the basin floor is believed to be no more than about 450 m deep throughout the area delineated by Fig. 1 (Subsurface Surveys, 1990). The three sites occupied by the present seismic surveys are located above the concealed basement ridge (Fig. 1b, Line 2) and directly adjacent to exposed granitic rocks at the Upper and Lower Narrows (Fig. 1b, lines 1 and 3). Basement rocks accordingly can be expected to lie at shallow or moderate depths beneath these sites.

The alluvial fill of the Victorville basin has been studied in detail at the southern margin of the basin near Cajon Pass (summarized in Meisling and Weldon, 1989), and at the former George Air Force Base (GAFB) northwest of Victorville (IT Corporation, 1992; Montgomery Watson, 1995; Chrisley, 1997; Sibbett, 1999). In addition, the U.S. Geological Survey is currently studying northerly parts of the basin near Victorville and GAFB by mapping surficial alluvial deposits and by investigating samples and drilling records from pre-existing water wells and exploratory boreholes (Cox and others, 1998; Cox and Tinsley, 1999; B. Cox, J. Hillhouse, and R. Forester, unpub. data). The following stratigraphic summary integrates the results of previous and ongoing geologic research.

The upper levels of the basin fill penetrated by boreholes near Victorville and GAFB consist of three main stratigraphic units: two thick layers of alluvial sand and gravel, separated by a thin layer of olive-gray to yellowish-brown lacustrine silt and clay (Chrisley, 1997; Sibbett, 1999; Cox and Tinsley, 1999). By interpolating between boreholes located south and west of the study area, the thicknesses of the upper alluvial unit and medial lacustrine unit are estimated to be roughly 175 m and 30 m, respectively, near the southwest corner of Fig. 1b. The reference boreholes do not penetrate to the base of the alluvial fill. However, if the maximum depth to local basement is roughly 450 m, as suggested by the previously described gravity studies, then the lower alluvial unit here could be as much as 250 meters thick. The thickness of the alluvial sequence presumably decreases to the north and east across the study area, toward the basement outcrops at the Lower and Upper Narrows.

From lateral and vertical variations in detrital composition, it is evident that the alluvial fill was derived from multiple sources on opposite

sides of the Victorville basin. The lower alluvial unit includes detritus of volcanic and metamorphic rocks that can be traced to sources north of the Victorville region. Southward-draining streams and alluvial fans deposited this material on the north flank of the basin. By contrast, the upper alluvial unit at Victorville and GAFB consists almost exclusively of granitic detritus that was transported northward from sources in the San Bernardino Mountains. Fluvial textures indicate this material was deposited by a Pliocene-Pleistocene precursor to the Mojave River (Cox and others, 1998; Sibbett, 1999; Cox and Tinsley, 1999). A thick mass of sand and gravel derived from the San Gabriel Mountains-the Victorville fan deposits of Meisling and Weldon (1989)-underlies the broad alluvial slope between Cajon Pass and Victorville, directly southwest of the study area. These old alluvial fan deposits accumulated contemporaneously with the fluvial deposits of the ancestral Mojave River as the adjoining fan and river constructed a composite alluvial wedge on the south flank of the Victorville basin. The underlying unit of lacustrine silt and clay contains tongues of sand derived from either side of the basin, reflecting an origin within a lake or wetland at the topographic center of the basin.

The overall stratigraphic configuration of the basin fill at Victorville and GAFB was controlled by the tectonically ascendant Transverse Ranges, which delivered a glut of alluvial sediments to the south flank of the Victorville basin, forcing the basin axis to shift northward with time. The upper-alluvial unit is markedly wedge shaped in cross section, with its thickness decreasing steadily from about 240 meters at southernmost Victorville (near Bear Valley Road) to 55 meters at the north end of GAFB. Furthermore, magnetostratigraphic and microfossil data from borehole cores at GAFB show that the age of the underlying lacustrine unit decreases laterally from late Pliocene, at the southeast corner of the base, to early Pleistocene at the northwest corner (B. Cox , J. Hillhouse, and R. Forester, unpub. data). These relations show that strata in the northern half of the Victorville basin accumulated time-transgressively, with the lacustrine unit lapping northward onto the lower alluvial unit and in turn being overlapped from the south by the upper alluvial unit. A similar diachronous sequence of alluvial and lacustrine deposits fills the East Antelope basin to the west (Dutcher and Worts, 1963, fig. 3; Londquist and others, 1993). The asymmetric filling of the Victorville and East Antelope basins resulted from uplift of the San Bernardino and San Gabriel Mountains relative to the southern Mojave Desert during the Pleistocene and late Pliocene (roughly the past 3 million years).

The filling of the Victorville basin was followed by an episode of stream incision in the late Pleistocene and Holocene. This is when the Mojave River eroded its modern canyon, including the bedrock gorges at the Upper and Lower Narrows. The broad floodplain of the ancestral Mojave River was stranded by this event, and its dissected remnants now form an elevated alluvial platform at Victorville and GAFB-the "George surface" of Cox and Tinsley (1999). River deposits that cap the George surface directly

north of GAFB were recently dated at about 60-70,000 years, based on optically stimulated luminescence (OSL) of detrital quartz grains (K. Ruppert and L. Owen, written commun., June 1999). If the OSL age accurately records the depositional age of the capping river deposits, then it simultaneously constrains the maximum age of river incision near Victorville.

The Mojave River canyon is a steep-sided trough, typically about 1.2 km wide, but locally constricting to 100 m or less where the river cuts through resistant granitic bedrock at the Upper and Lower Narrows. The topographic relief between the active river channel and George surface is on average about 60 meters. The canyon was significantly deeper at certain times in the Holocene or latest Pleistocene, however. Borehole data show the base of the canyon is backfilled with at least 15 meters of unconsolidated Holocene alluvium near Victorville (P. Martin, oral commun., 1998). Thus, alluvial deposits beneath seismic lines 1 and 3 would be expected to consist of young alluvium deposited by the modern Mojave River after the bedrock channels were incised at the Upper and Lower Narrows.

Published geologic maps imply that the old, pre-incision alluvial fill of the Victorville basin is unfaulted and otherwise undeformed near the study area (Bowen, 1954; Dibblee, 1960; Bortugno and Spittler, 1986). The only geologic structure shown on these maps is a fault of indefinite age cutting granitic rocks northeast of the Upper Narrows (Victorville Fault of Bowen, 1954). However, given that the Victorville basin evolved adjacent to the Transverse Ranges as the latter were dynamically uplifted by compression along the San Andreas Fault (Meisling and Weldon, 1989), one might expect to find some evidence of faulting or folding within the Pliocene-Pleistocene-age basin fill.

During the present study, numerous geologic lineaments were identified near Victorville through inspection of aerial photographs (Fig. 1b). These linear features are defined by tonal contrasts, aligned topographic elements, and bands of vegetation. Most of them are short, discontinuous features that probably represent minor fractures or insignificant faults. However, several long, northwest-trending lineaments that intersect seismic line 2 have pronounced topographic expression and may represent important faults cutting the alluvial fill and underlying basement rocks of the Victorville basin. Some northeast-trending lineaments within the granitic rocks also appear to be fault related. These include the previously mapped Victorville Fault near the Upper Narrows, and another prominent lineament north of the Lower Narrows. An east-trending lineament within Pleistocene alluvium west of the Lower Narrows also is ascribed to faulting, as it coincides with a ground-water barrier at Turner Springs and is marked by steep northward-dipping shear planes about 0.6 km west of Turner Springs (B. Cox, unpub. mapping).

Seismic Surveys

Seismic refraction and seismic reflection surveys provide complimentary information about the subsurface. Seismic refraction surveys

measure the velocity at which seismic waves travel through the subsurface. This is useful information because correlations can be made relating possible subsurface composition, water saturation levels, and seismic velocities (Nur, 1982; Catchings and Lee, 1996; Christensen, 1996; Mavko et al., 1996). Although it is not possible to determine the exact composition on the basis of velocity information, it is possible to differentiate principal subsurface composition, such as solid crystalline rock versus unconsolidated sedimentary rock or unconsolidated sand versus saturated clays. Seismic reflection surveys provide reflection images of the subsurface. The interface between differing types of subsurface layers typically results in a velocity or density discontinuity. Seismic energy reflects from such interfaces and can be plotted in a manner to produce an image of the subsurface. Subsurface images of discontinuities between layers is useful because it is possible to laterally "map" subsurface stratigraphic horizons and structures, such as faults, folds, pinchouts, etc. By combining seismic refraction and reflection surveys into one survey (referred to here as seismic reflection-refraction surveys), it is possible to place many constraints on the subsurface in areas of interest. The surveys presented in this report utilized both seismic refraction and seismic reflection imaging techniques.

Seismic Data Acquisition

From December 1997 through February 1998, three high-resolution seismic reflection/refraction profiles, ranging in length from approximately 68 m to about 2800 m, were acquired within the city of Victorville, California (Fig. 1b). In this report the seismic profiles are referred to as Lines 1, 2, and 3. Comparative statistics among the seismic profiles are shown in Table 1. For each seismic profile, we utilized a shoot-through acquisition technique, whereby sensors and recording channels remained stationary as shots were fired through the actively recording array. Seismic sources consisted of a combination of downhole explosive sources (1 lb ammonium nitrate) and BETSY-Seisgun™ 8-gauge-shotgun blanks. Explosive shot holes were drilled to depths of approximately 2 m, and shotgun holes were drilled to depths of approximately 0.5 m. The data were recorded using a cabled array of Geometrics Strataview™ RX-60 seismographs and 40-Hz Mark Products™ geophones. A maximum of 240 channels was used in acquiring the seismic data. Prior to data acquisition, shot point and geophone locations for each seismic profile were surveyed using a measuring tape, and after the data were acquired, all locations were re-surveyed using an electronic distance meter (EDM) or a Global Positioning System (GPS) receiver. EDM-determined locations are estimated to be accurate to within 0.001 m, and GPS-determined locations can be as accurate as 0.0001 m (see Appendix A, B. and C).

Shot timing for the BETSY seisgun ™ was determined electronically at the seismic source when the hammer electrically closed contact with the BETSY seisgun ™. For ammonium nitrate charges, both the seismic source and the seismograph were simultaneously triggered by synchronized

electronic master clocks (1 ms accuracy) that were calibrated daily by satellite.

Line No.	Orientation	Length (m) of Geophone Line	Length (m) of Shot Line	No. of Shots	No. of CDP's	Max Fold
1	NE-SW	59.0	68	69	133	60
2	NE-SW	2497.35	2547.18	498	1057	229
3	NW-SE	881.86	926.65	180	365	177

Table 1. Acquisition parameters for seismic lines

During data acquisition, the seismic data were recorded on the hard drive of the Geometrics seismograph systems in SEG-2 format and subsequently downloaded each night to 4mm tape in SEG-Y format.

Line 1

Line 1 consisted of a 68-m-long, NE-SW-trending profile that crossed the Mojave River at the Upper Narrows (Fig. 1b). Because of the relatively short length of the seismic profile, only one RX-60 seismograph, with 60 live channels, was deployed, and it remained stationary during data acquisition. Geophones were spaced approximately 1 m apart and varied in elevation by no more than 2 m across the seismic profile (Fig. 2). Relative to the end points of the seismic profile, the array of geophones did not vary from a straight line (Fig. 3). The close spacing of geophones and shot points allows for high resolution of the subsurface, and the limited change in elevation does not require special processing measures. In theory, a straight line is desirable so that artifacts that are unrelated to the subsurface structure are not generated by the geometry of the line.

The seismic sources, generated by seisgun blanks, were fired in approximately 0.5-m-deep holes. Shot points were co-located with the geophones at 1-m spacing, and each shot point was laterally offset from the corresponding geophone by 1 m. However, a few additional shot points extended beyond the ends of the geophone array, with a total of 69 shots used. Shot point elevations varied by less than 3.5 m across the seismic profile (Fig 4), and the shot points formed an approximately straight line relative to the endpoints of the array (Fig. 5).

Fold (the theoretical number of times a reflection point is sampled at a given location) along Line 1 was smoothly varying because of the stationary recording array (Fig. 6). Maximum folds of approximately 60 were obtained in the center of the seismic profile, decreasing to about 1 at the ends of the line. Because the fold is greatest in the middle, the most reliable reflection images for the deeper structure should be in the middle of the seismic profile. However, because the targets of interest were relatively shallow (<300 m), low fold on the ends of the seismic profile was of little concern, as our previous studies have shown that folds above about 30 are reliable to depths of approximately 350 m when using the BETSY Seisgun ™ source, as was used on line 1.

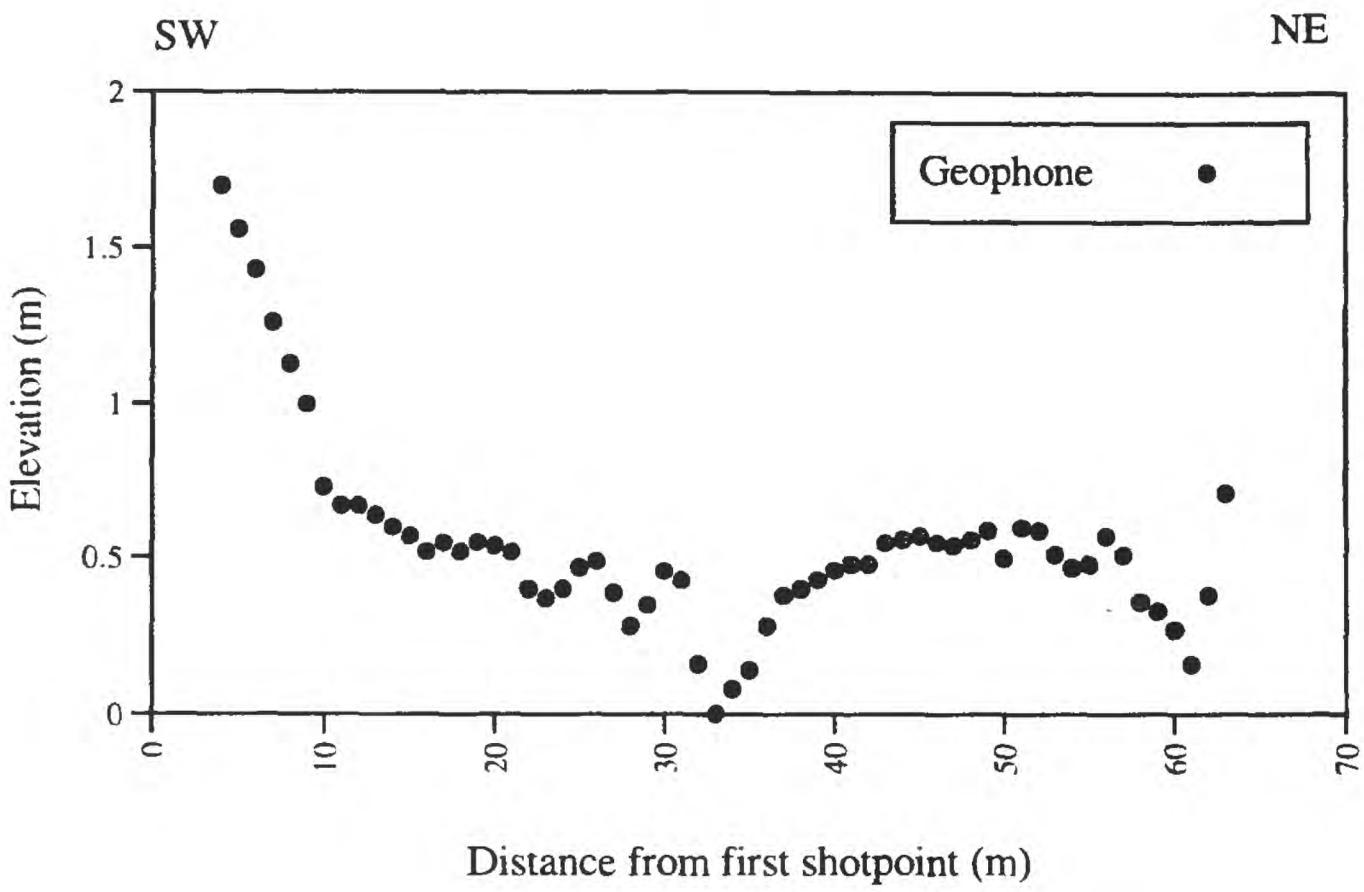

Fig. 2. Geophone elevation along Line 1. Geophone elevation is relative to the topographically lowest geophone.

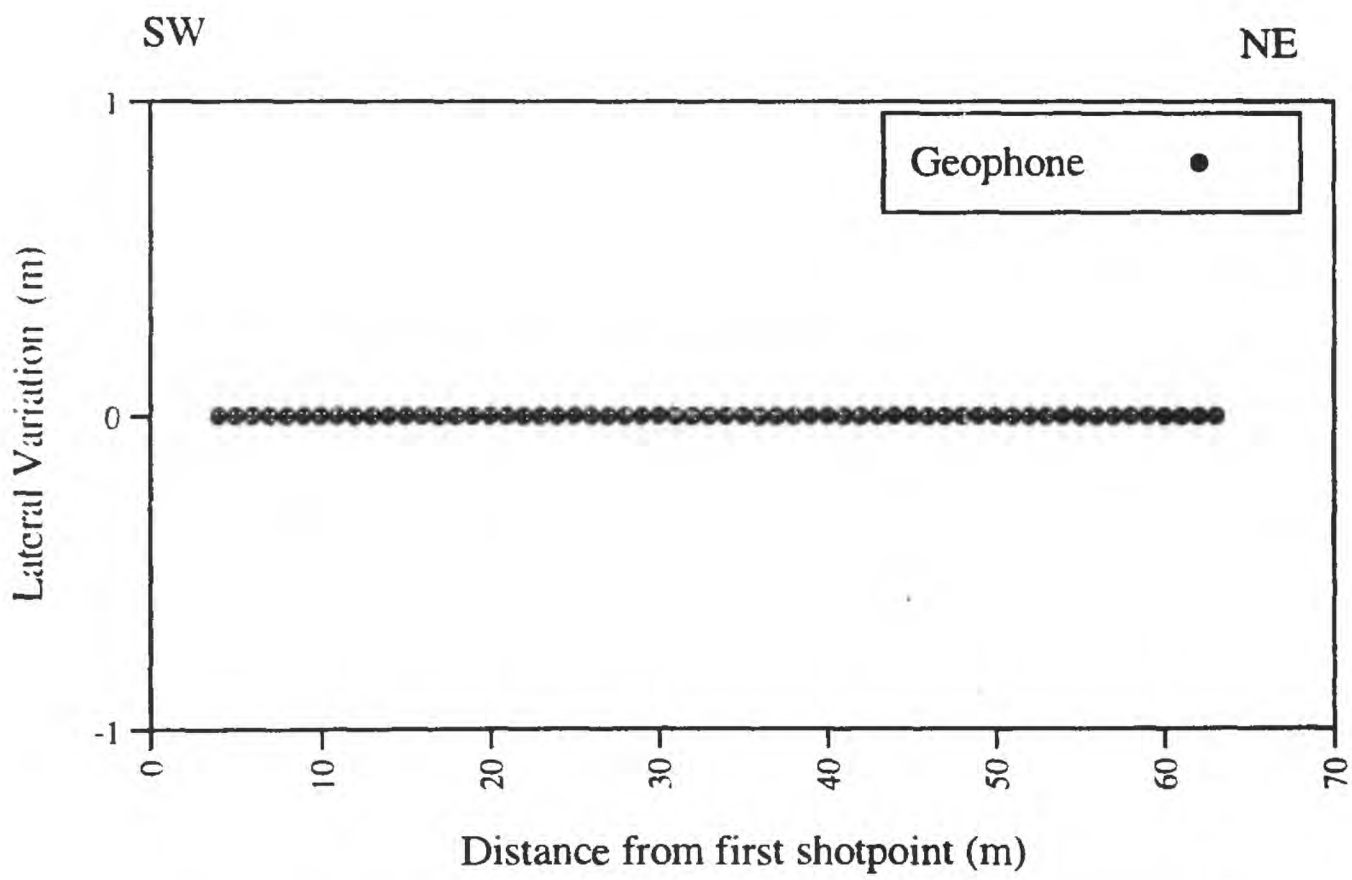

Fig. 3. Geophone variation from a straight line connecting the first amd last geophones along Line 2.

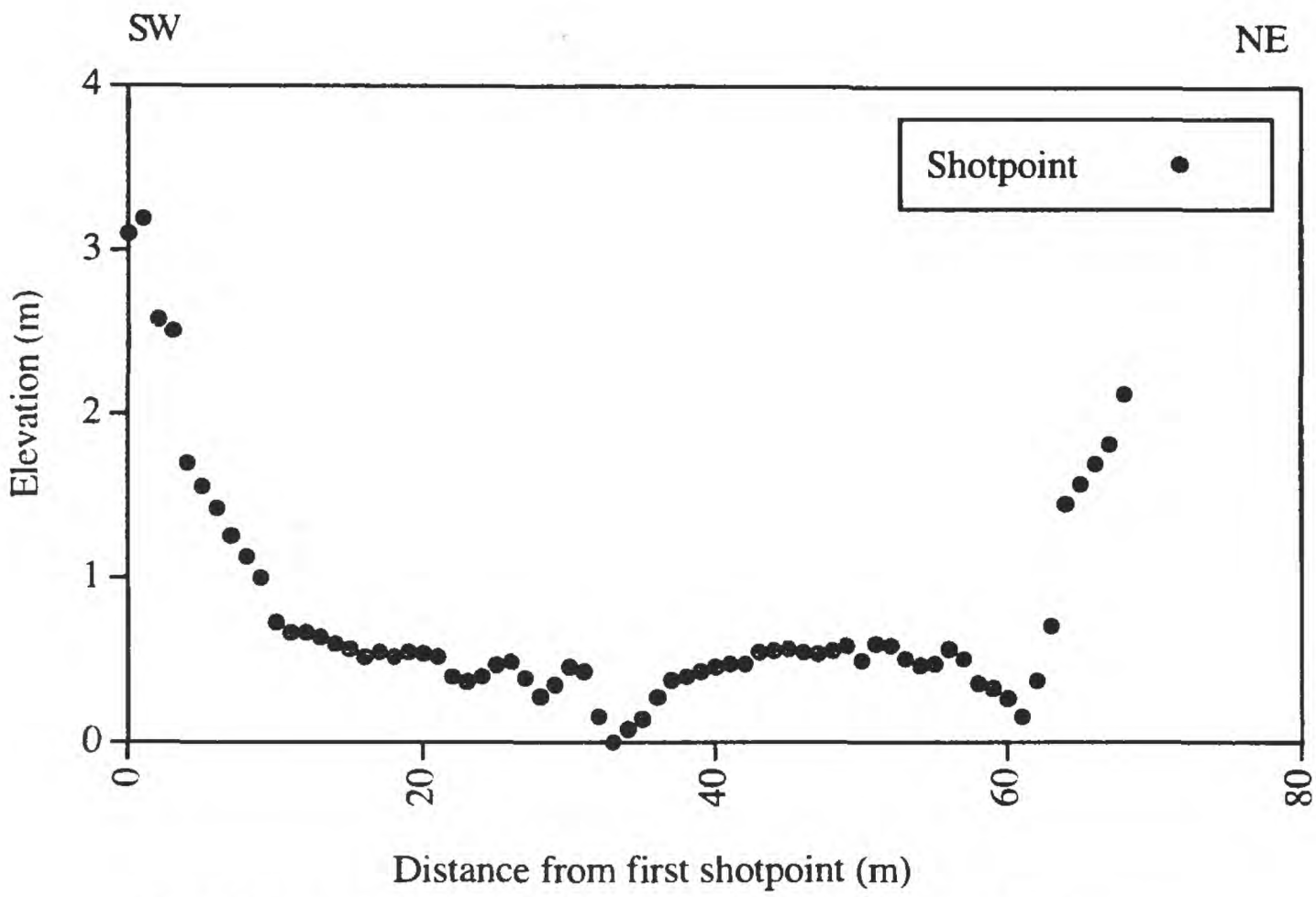

Fig. 4. Shotpoint elevation relative to the topographically lowest geophone.

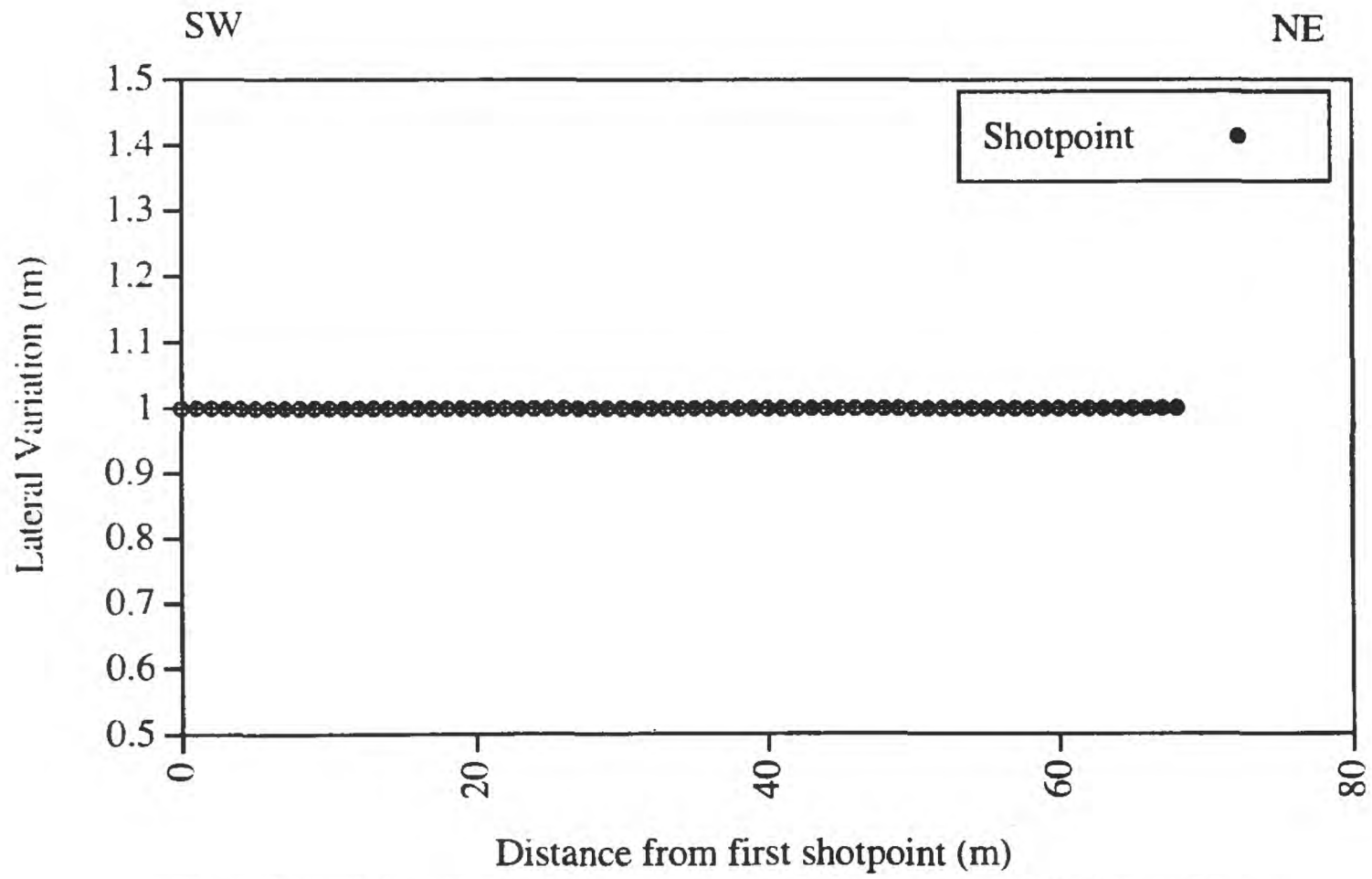

Fig. 5. Lateral shotpoint variation from a straight line connecting the first and last geophone.

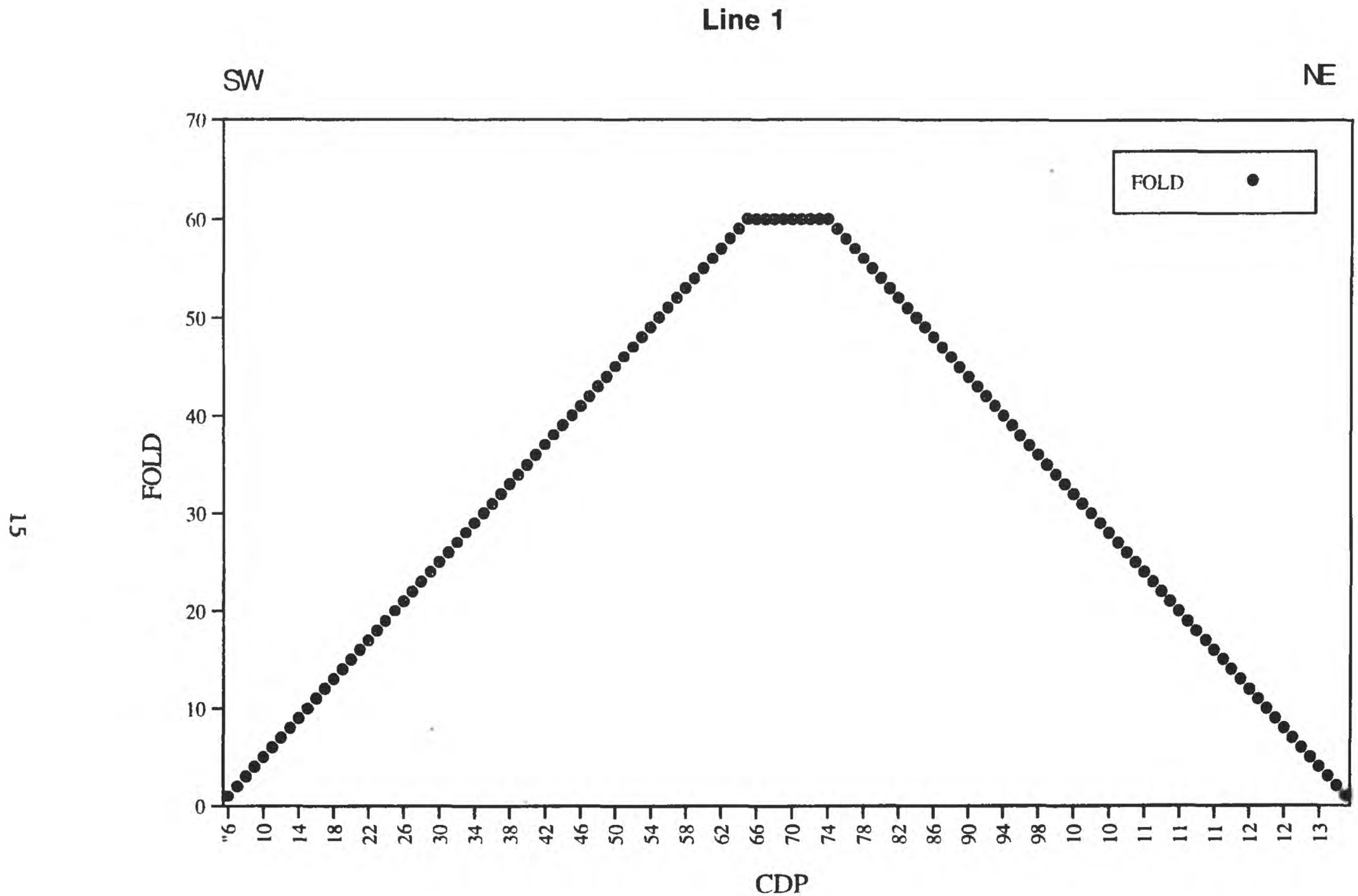

Fig. 6. Variation in fold as a function of Common Depth Point (CDP) along Line 1.

Line 2

Line 2 consisted of a 2500-m-long, NE-SW-trending profile that terminated southwest of the Mojave River at California State Highway 18 (Fig. 1b). The seismic profile was located within the city limits of Victorville along an easement owned by the Los Angeles Department of Water and Power. The seismic profile originated from the southwest with a 1500-m long continuous array of geophones, with each geophone spaced 5 m apart. Five Geometrics RX-60 Strataview™ seismographs, with a total of 300 live channels, were used to record the seismic signals sensed by the geophone array. The geophone array remained stationary until shots were fired at the first 150 shotpoints. Thereafter, 60 geophones were moved to the northeast end of the array, and an additional 60 shots were fired. This process was repeated until the end of the seismic line was reached. As with Line 1, we used Mark Products™ 40-Hz, single-component geophones to sense the ground motion. Geophone elevations along the geophone array varied by approximately 30 meters over the 2500-m-long profile (Fig. 7). Relative to a straight line connecting its end points, the geophone array formed an approximately straight line, varying laterally by only about 2.5 m over the entire 2500+ m length of the array (Fig. 8).

Seismic sources were generated by ammonium nitrate explosions in 2-m-deep holes that were spaced every 10 m and by alternating BETSY Seisgun ™ blanks at about 0.5 m depth, spaced every 10 m. Thus, the combination of explosives and blanks generated a seismic source approximately every 5 m that was co-located with and offset from a geophone by 1 m. Shot point elevations along the profile varied by about 30 m in a manner similar to that of the geophones (Fig. 9). Relative to a line connecting its endpoints, the shot point array formed an approximately straight line that varied laterally by less than 4 m over a distance of 2500 m (Fig. 10).

Fold along Line 2 varied with distance along the seismic profile, ranging from about 12 near the ends of the array to about 229 at approximately one-fourth and three-fourths the length of the seismic profile (Fig. 11). This variation in fold was caused by the movement of geophones during data acquisition, as described above. In practice, we have found that folds of 1 can generate reliable data for depths in excess of 1 km when using small explosive sources. Therefore, reflectors of interest to this study should be reliably imaged at all locations along the profile.

The relatively straight arrays of geophones and shotpoints, combined with the high folds, suggest that the data are not likely to have image artifacts generated by the geometry or acquisition techniques. The elevation and other geometrical variations were included in the processing steps.

Line 3

Line 3 is an approximately 925-m-long, SE-to-NW-trending profile that originated at Lower Narrows at Highway 18 and the Mojave River (Fig. 1b). Most of Line 3 was located within the Mojave River channel and crossed the actively flowing channel of the Mojave River. Three Geometrics

Line 2

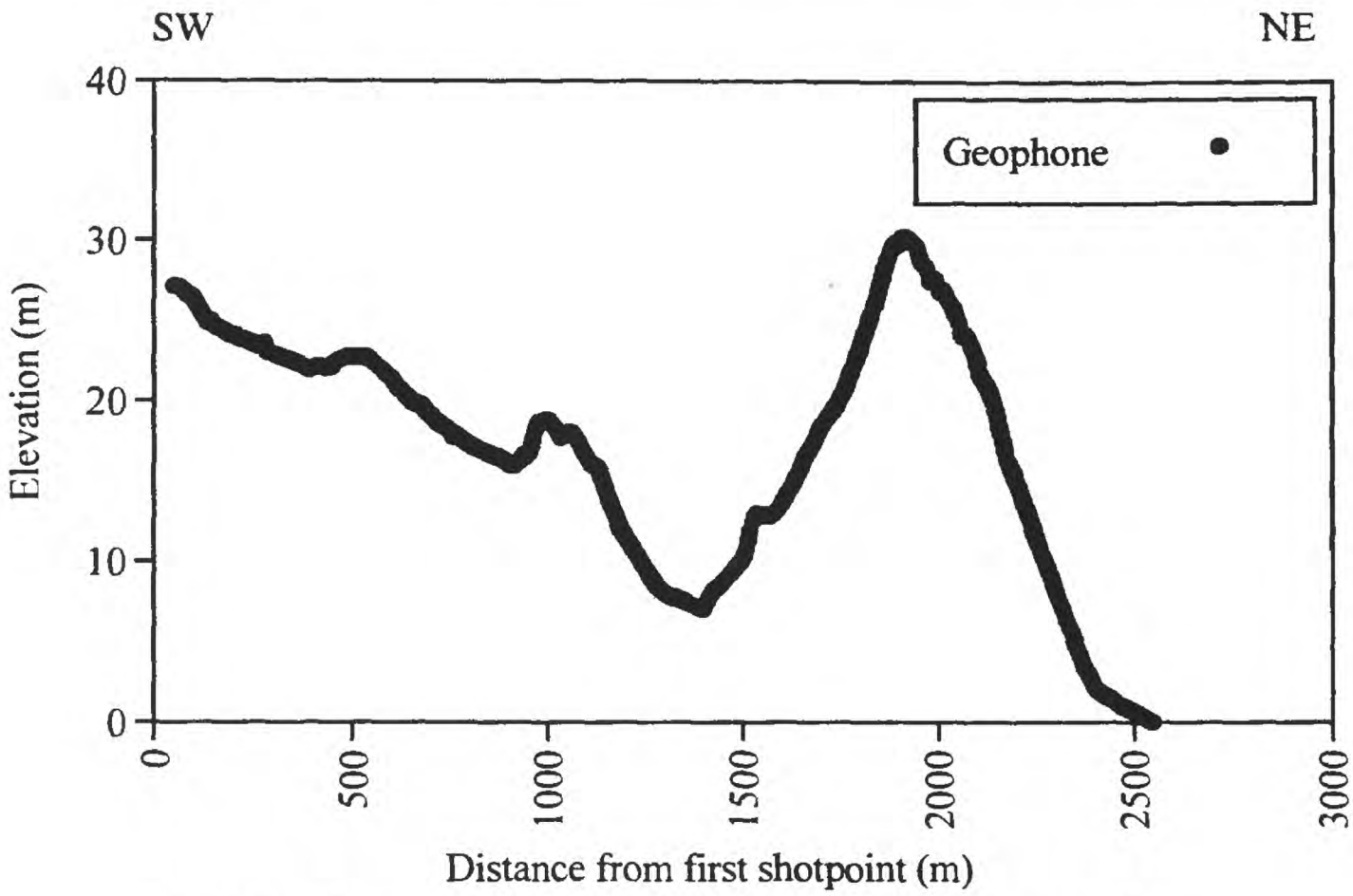

Fig. 7. Geophone elevation relative to the topographically lowest geophone.

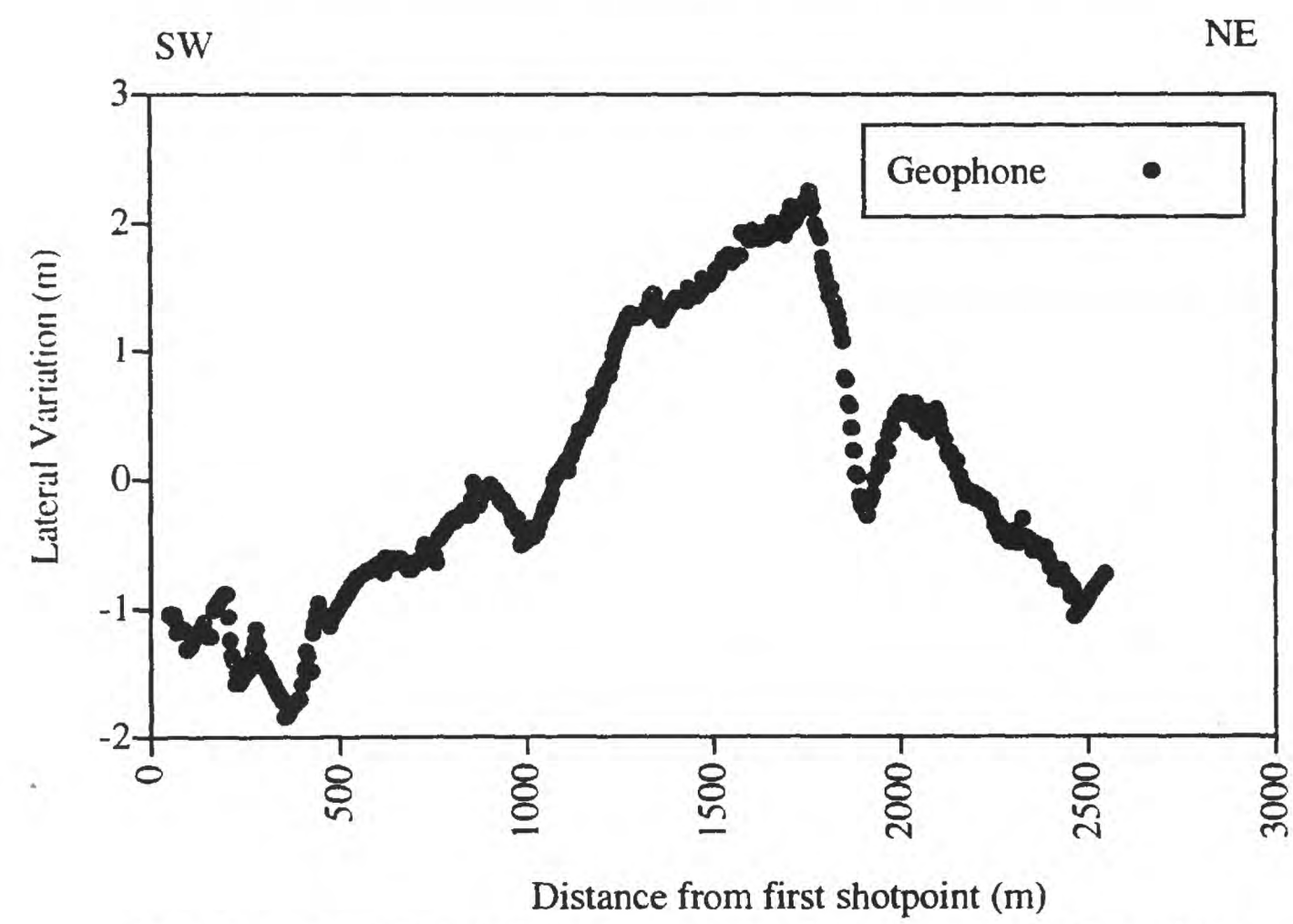

Fig. 8. Lateral geophone variation from a straight line connecting the first and last geophones.

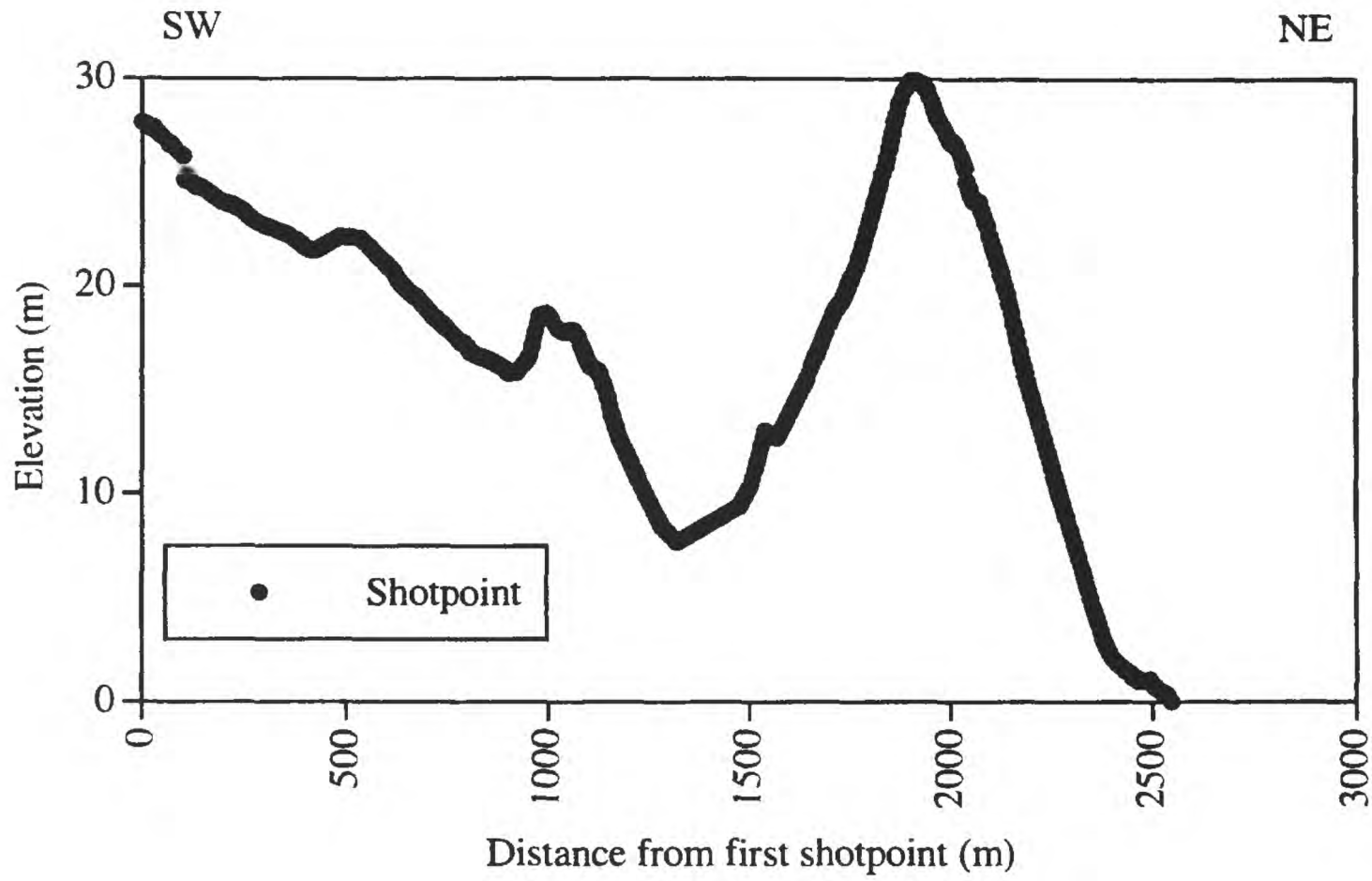

Fig. 9. Shotpoint elevation relative to the topographically lowest shotpoint.

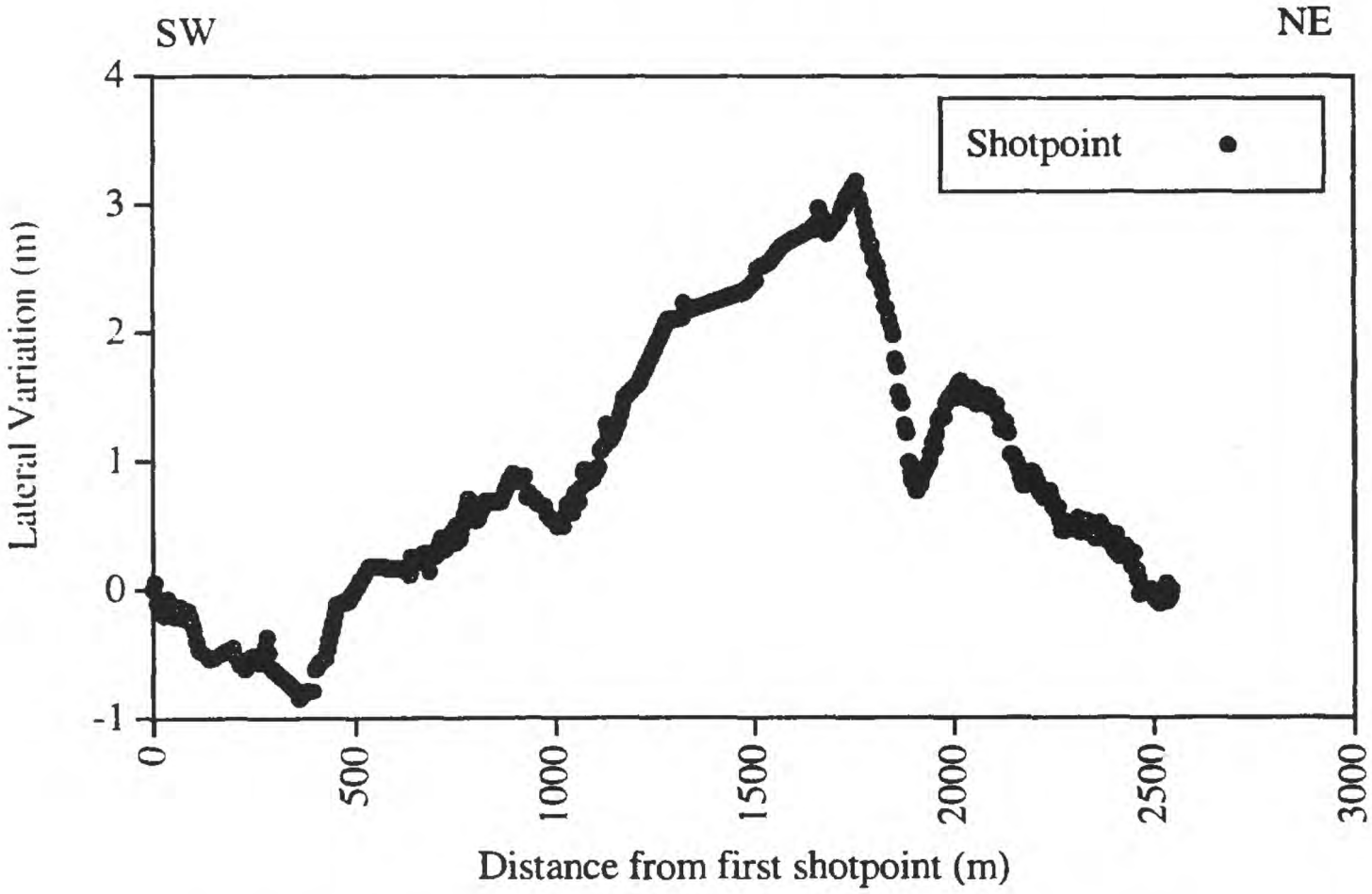

Fig. 10. Shotpoint variation from a straight line connecting the first and last shotpoints.

Fig. 11. Variation in fold as a function of Common Depth Point (CDP) along Line 2.

Strataview™ RX-60 seismographs, with a total of 180 live channels, were utilized and remained stationary during data acquisition.

Mark Products™ 40-Hz, single-element geophones were connected by cable and spaced approximately 5 m apart along the recording array. Geophones elevations varied by less than four meters within the river channel (Fig. 12) but laterally varied by as much as 9 m from a straight line that connects its end points (Fig. 13). Although this variation from linearity is only about 1% of the length of the seismic array, the 9-m variation could possibly cause depth-calculation errors of about 1 m in the shallow (upper 50 m) section. Thus, although minor, this possible error must be considered in interpreting the seismic section. Seismic sources were generated by 300-grain BETSY Seisgun™ blanks in 0.5-m-deep holes. Shot points were co-located and laterally offset approximately 1-m from the geophones along the recording array. Additional shot points were positioned at the ends of the recording array to increase the fold there. Shot points varied by more than 3 m in elevation over the length of the array (Fig. 14) and laterally varied by as much as 10 m from a straight line (Fig. 15). This variation in linearity of the profile could cause depth-calculation errors of about 1 m.

Fold along Line 3 was smoothly varying, ranging from approximately 1 near the ends of the profile to nearly 180 near the center of the profile (Fig. 16). The smooth variation in the fold suggests that there should be clear images across the seismic profile within the depths of interest to this study.

Seismic Data Processing

Because both seismic reflection and refraction data were simultaneously acquired, both types of data can be independently processed, interpreted, and compared.

Refraction Velocity Analysis

To determine the velocity structure of the shallow subsurface, we used a tomographic inversion technique developed by Hole (1992). This technique is a computerized inversion scheme that compares observed and calculated travel times from thousands of raypaths to measure the velocity along the seismic profile. Within the model, velocity measurements are made along a grid that depends largely on the shot and geophone spacing and the resolution is similar to the larger of the two. For the profiles presented here, the shot and geophone spacing are the same; thus, depth determinations are resolved to within about 1 m for Line 1 and about 5 m for Lines 2 and 3. The maximum depth of velocity measurement is related to the length of the live channels. For Line 1, we obtain little velocity information below about 30 m depth. Along Lines 2 and 3, tomographically derived velocity information is limited to depths above about 300 m and 100 m, respectively.

To obtain velocities at greater depths than those obtained by inversion techniques, we used semblance and hyperbolic techniques and apriori knowledge of the subsurface. However, for depths of interest to this study, velocities were obtained from the inversion techniques.

Line 3

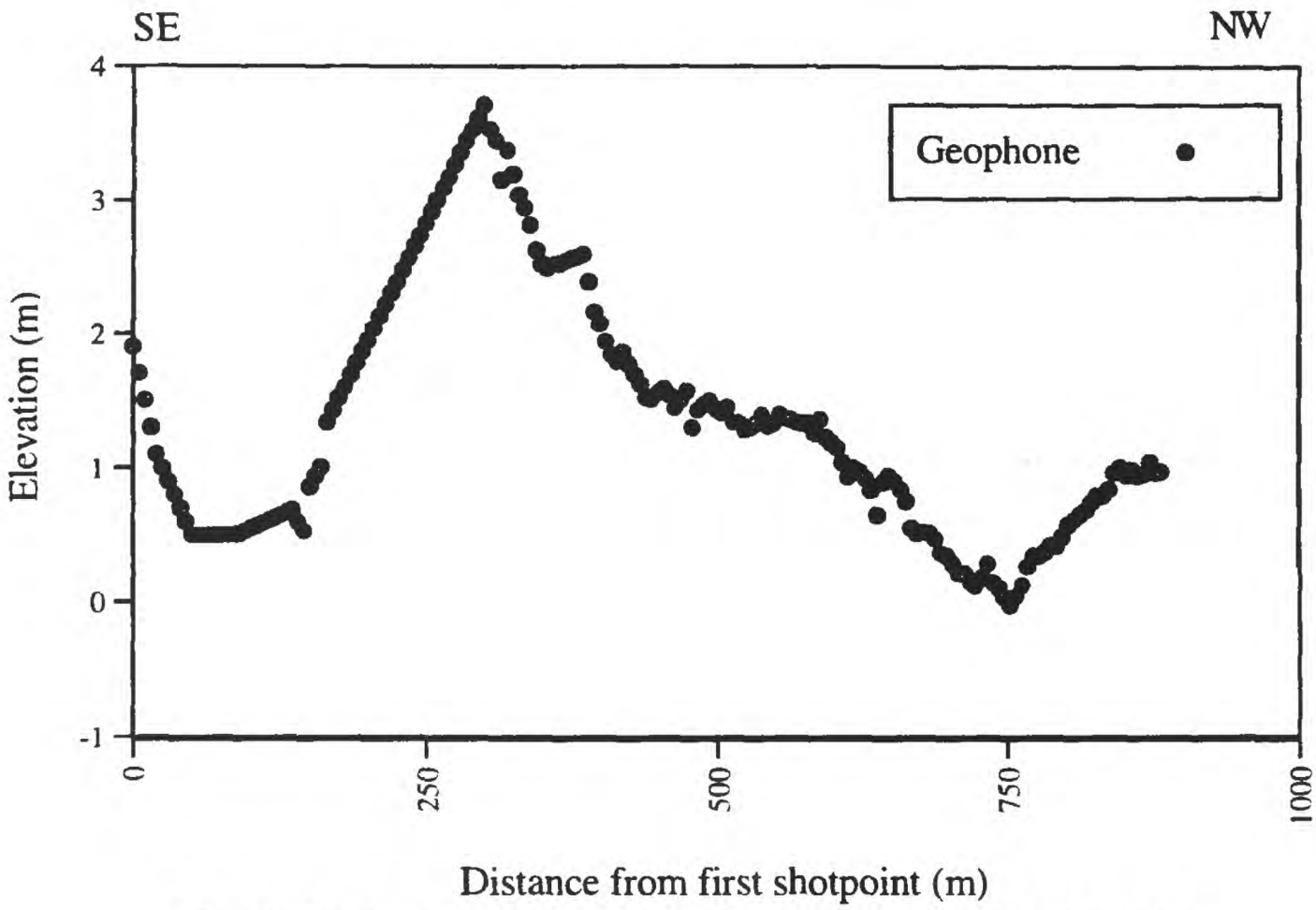

Fig. 12. Geophone elevation relative to the topographically lowest geophone along Line 3.

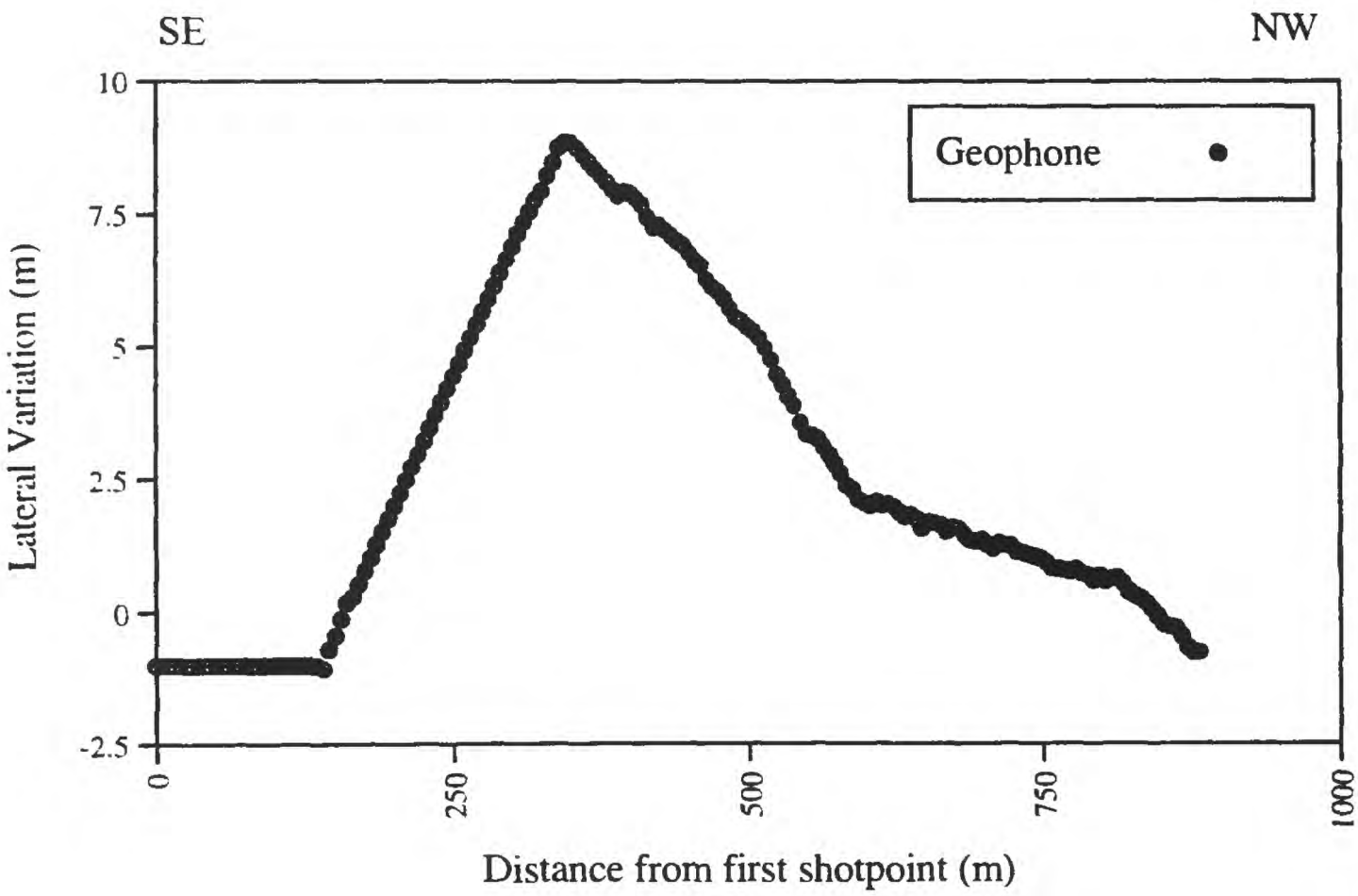

Fig. 13. Geophone variation from a straight line connecting the first and last geophones.

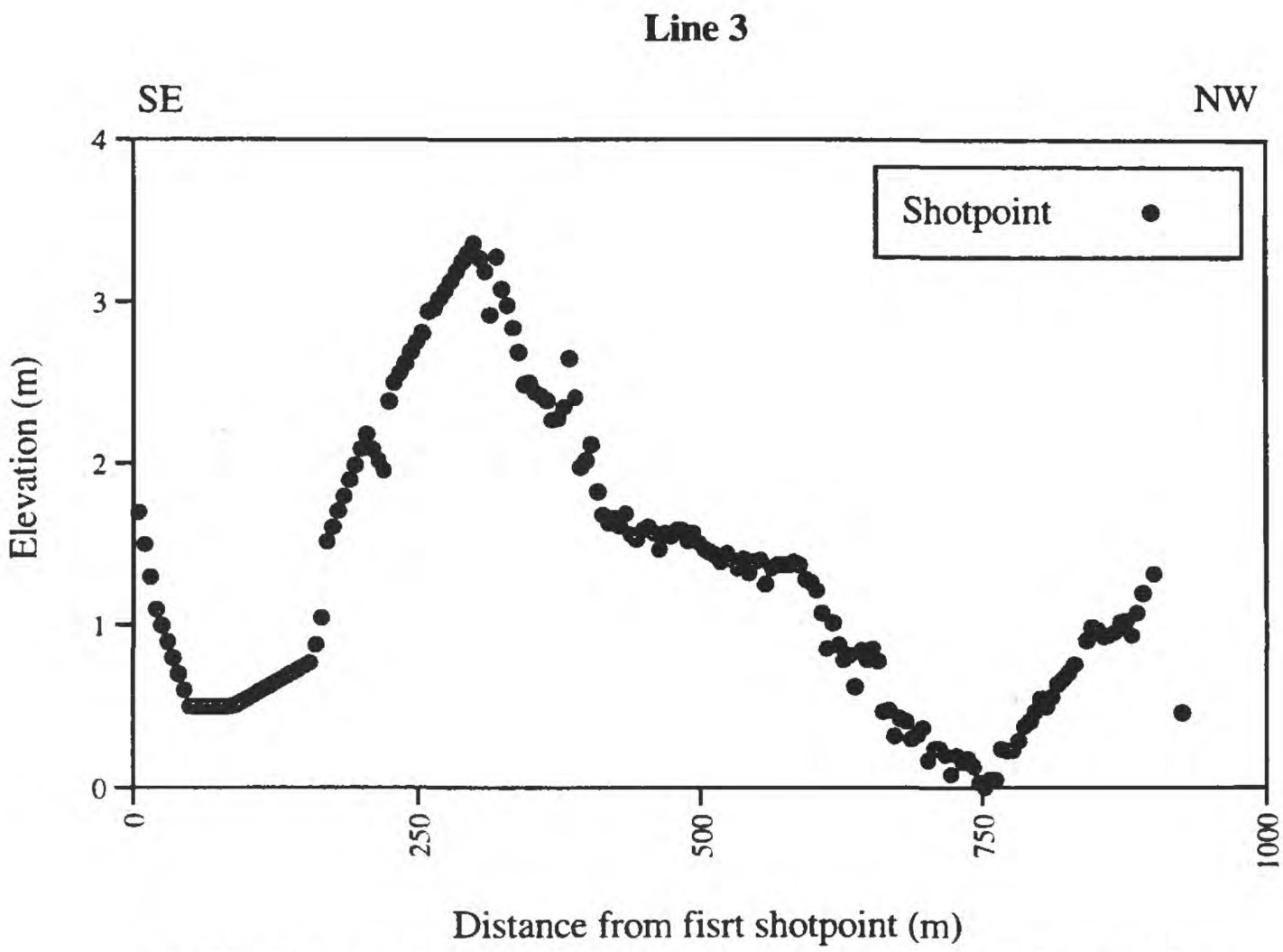

Fig. 14. Shotpoint elevation relative to the topographically lowest shotpoint along Line 3.

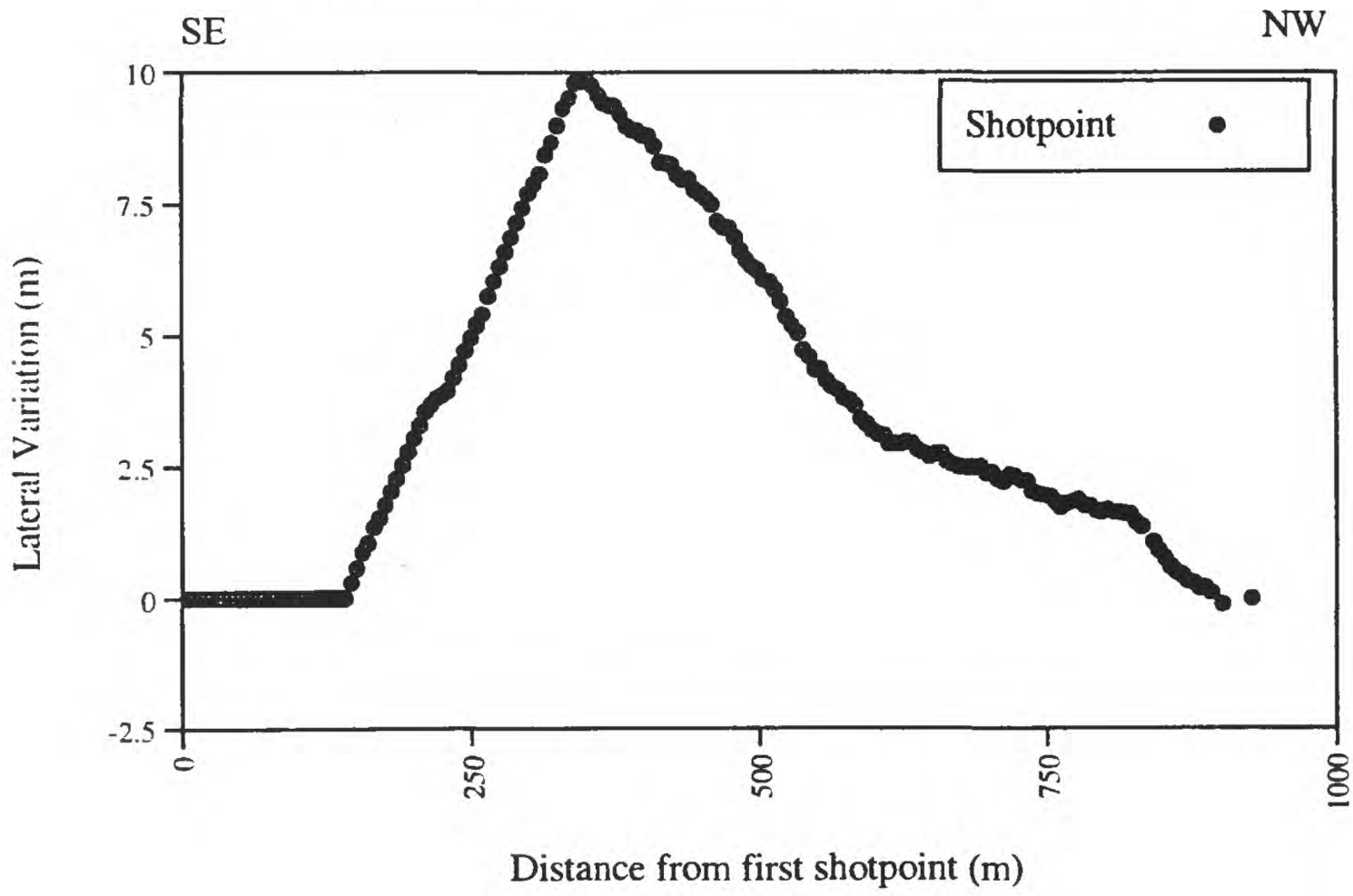

Fig. 15. Shotpoint variation from a straight line connecting the first and last geophones.

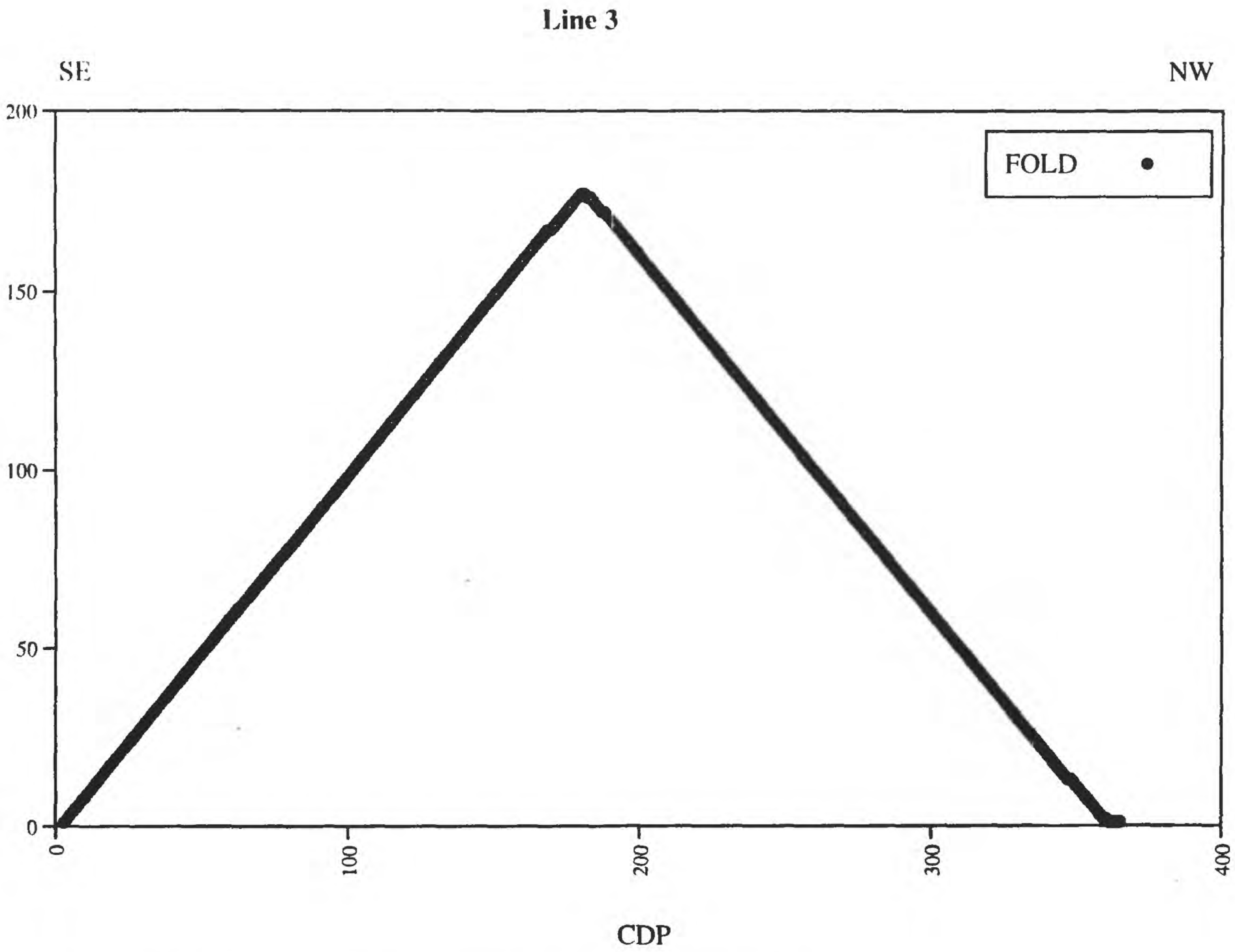

Fig. 16. Variation in fold as a function of Common Depth Point (CDP) along Line 3.

Seismic Reflection Processing

Seismic reflection data processing was accomplished on a Sun Sparc 20™ computer using an interactive seismic processing package known as Promax™. The following steps were involved in data processing:

Geometry Installation

Lateral distances and elevations described above were used to define the geometrical set up of each profile. We installed the electronically-measured geometries into the Promax processing package for each profile separately so that we could account for shot and receiver elevations and locations in the processing routine.

Trace Editing

Occasionally, poor coupling between the geophones and the ground, malfunctioning geophones, or cultural noises close to the geophones resulted in unusually noisy traces that were edited for those locations. However, such traces were not necessarily unsuitable for all shot gathers; therefore, independent trace editing was employed for each shot gather.

Bandpass Filtering

Most of the data of interest for seismic imaging and velocity measurement are well above 15 Hz, and most of the undesirable seismic data, such as surface waves and shear waves, are well below 15 Hz. Therefore, a bandpass filter with a low cut of 15 Hz was used to remove most surface and shear waves as well as cultural noise.

F-K Filtering

Not all surface waves were removed by simple bandpass filtering. To remove those surface and air waves that were not removed by bandpass filtering, we used a FK filter. In seismic reflection data processing, we used trace muting to remove first-arrival refractions.

Timing Corrections

Although the shotgun source electronically triggers the seismographs, there are small (~2 ms) delays between the electrical trigger and the actual shotgun explosions. We corrected for the delays by removing a constant 2 ms from the start time of each shotgather.

Velocity Analysis

Velocities in the shallow section (~1 m to ~150 m) were determined using velocity inversion techniques, but velocities in the deeper section were determined using shotgathers and CDP stacks.

Elevation Statics

Elevation statics were also employed to correct for variations in elevations by using the electronically-determined locations and inversion-determined velocities.

Moveout Correction

Due to progressively greater traveltimes for the seismic waves to reach sensors that were progressively farther from each shotpoint, there was a delay (moveout) for each seismic arrival on the seismic record. To sum (stack) the data at each location, this moveout was removed.

Velocity Inversion

As described above, velocities were measured from the seismic data using a computerized inversion routine.

Muting

To remove refractions and other arrivals that were not completely removed using filtering techniques, we used trace muting before and after stacking.

Stacking

To enhance the seismic signal at each location, individual reflections were summed together in a process called stacking.

Migration

Due to the presence of numerous faults and diffraction points in the subsurface, diffraction hyperbolae were observed throughout the section. Where necessary, we used pre-stack migration in selected sections to collapse the diffraction hyperbolae to better identify the major faults.

Interpretation

Line 1

Interpreted Reflection Section

Migrated seismic reflection and interpretative sections of the upper 100 m beneath Line 1 are shown in Fig. 17a. All discussions of depth in the interpretative sections refer to depth below the ground surface (bgs). These data show coherent reflections only at depths less than ~20 m beneath the surface, with most reflections discontinuing at about 15 m depth. The non-reflective rocks below about 15 m depths are probably quartz-monzonite rocks that crop out on either side of the profile, and thus, are not layered. Because the deepest reflections vary along the profile, we suggest that bedrock varies laterally between about 12 and 20 m. The most laterally continuous reflectors appear to be in the upper 5 to 10 m, which may suggest continuous sand layers across the profile in that depth range.

In 1905, the US Geological Survey drove several test wells in the general vicinity of Line 1 to determine the quantity of underflow through the "upper narrows" (Slichter, 1905). The maximum depth to bedrock was measured at 14 m (46 ft) below ground surface, which compares well with our discontinuous reflectors at 15 m across most of the profile. Slichter's (1905) survey found that at depths below 8-9 m (25-30 ft) the unconsolidated deposits consisted of low-permeability silty gravel deposits, which is also consistent with the maximum depth of laterally continuous reflectors (10 m) on the seismic image.

Although it is difficult to interpret faulting and fracturing along the line, layers below about 5 m appear to be vertically offset, suggesting that the river may follow a zone of faulting or fracturing in the basement rocks (Fig. 17c). Correlation with the seismic refraction data provides further constraints on the depth to crystalline rocks.

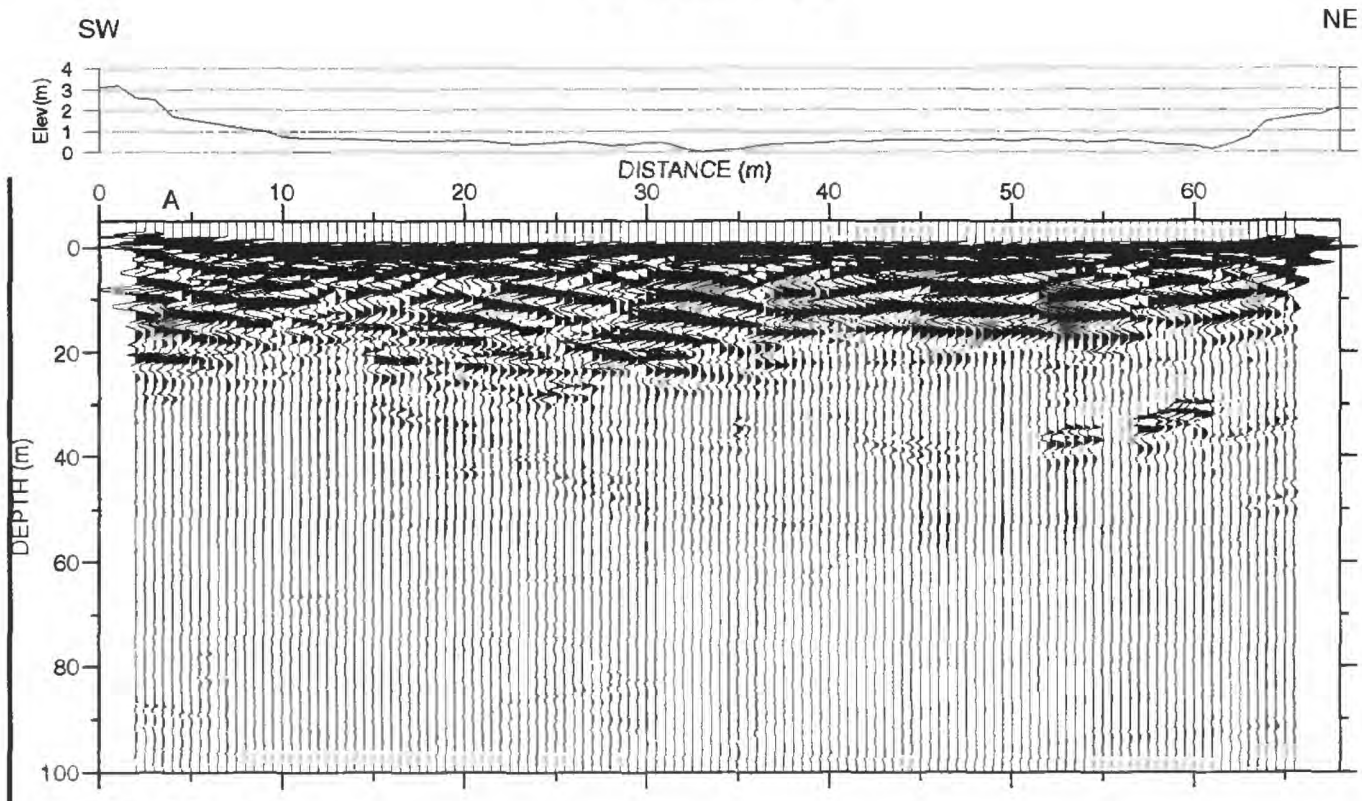

Fig. 17. Stacked seismic

2 agc = 15, tk = 90-400, 1-600, 50% bp = 200-400-800-1600
poststack bp = 150-300-800-1600, agc = 500

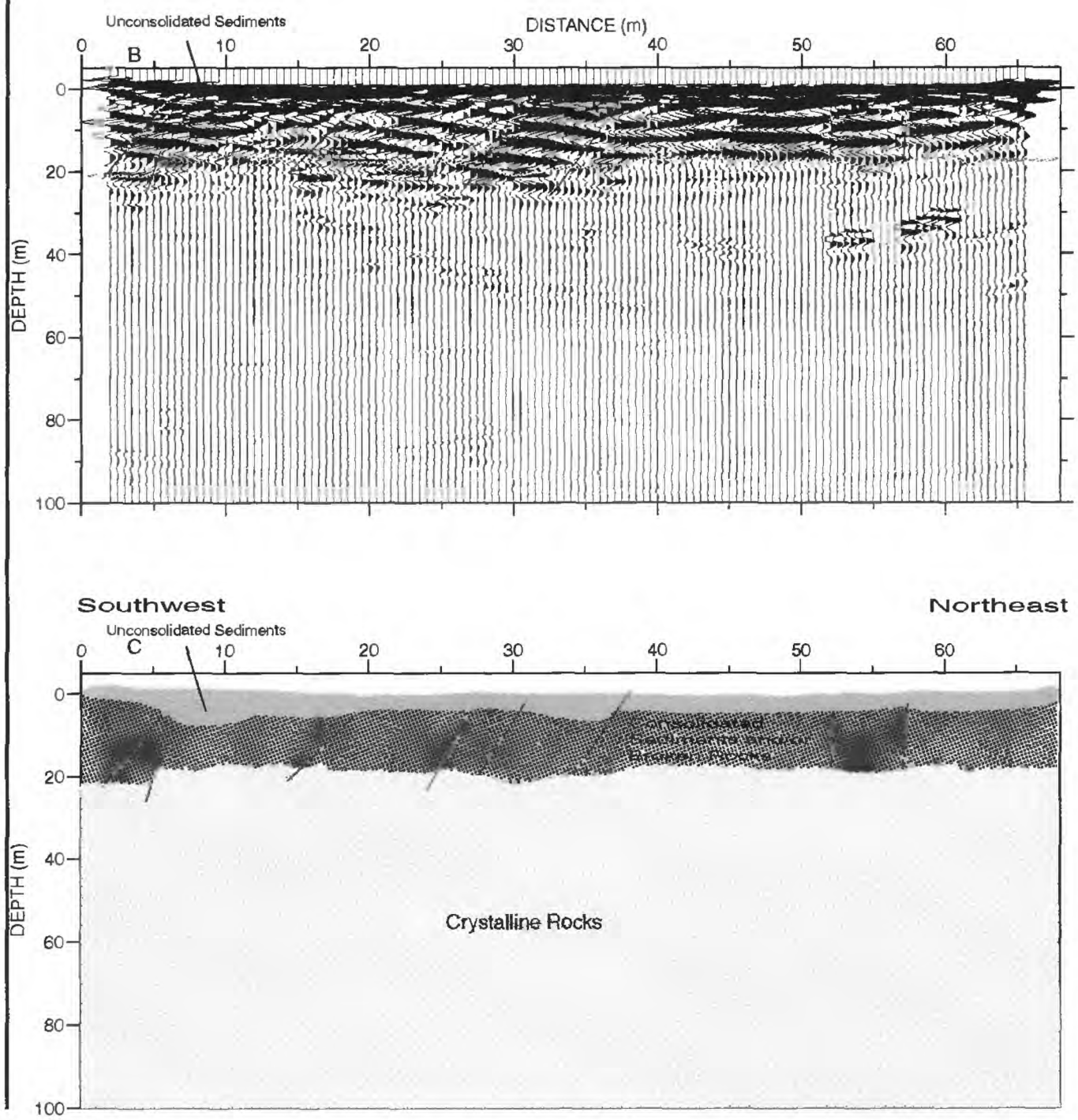

Fig. 17 (a) Uninterpreted seismic reflection image for Line 1. (b) Interpreted seismic section for Line 1. Yellow layers are interpreted to be unconsolidated sediments and the underlying reflective layers are interpreted to be consolidated sediments, clays, or broken rocks. The non-reflective section below about 20 m depth is interpreted to be crystalline rocks, such as granite. (c) Interpreted cross section along line 1.

Interpreted Refraction Section

Seismic velocities along Line 1 range from about 600 m/s at the surface to about 6000 m/s at 25 m depth (Fig. 18). Velocities of about 1500 m/s which are consistent with water-saturated sediment, are less than about 2 m deep across most of the profile. Velocities less than about 3800 m/s (green and blue on Fig. 18) likely represent clays or highly fractured rock and are confined to the upper 10 m. Velocities of about 4000 to 5000 m/s (yellow on Fig. 18) are consistent with those expected for weathered or fractured basement. The 4000-to-5000 m/s velocity probably represents a 2-to-5-m thick weathered zone of the basement rocks at depths ranging from 14 m to 19 m. Velocities in excess of 5000 m/s probably represent the unweathered quartz-monzonite basement rocks that crop out near the ends of the seismic profile.

Combined Reflection and Refraction Sections

Combined reflection and velocity images of the subsurface along Line 1 are shown in Fig. 19. Most reflections are confined to the upper 15 m where velocities range from about 1000 m/s to less than 4000 m/s, these velocities are consistent with layered sediments. The higher velocities (>4000 m/s) are largely confined to the non-reflective subsurface, except a few reflections near the center of the profile. These reflections occur near the top of the higher velocity section and are laterally discontinuous. Such reflections may arise from reflected energy that originates out of the plane of the seismic profile or from cracks within the top of basement (quartz monzonite).

Line 2

Interpreted Reflection Section

An unmigrated, stacked seismic reflection image and an interpretation of the upper 1000 m along Line 2 are shown in Figs. 20 and b. The data show numerous reflections from the surface down to 1000 m depth. The upper 150 m depth along most of the profile consist of relatively thin reflectors that probably arise from unconsolidated to partially consolidated sediments. Within the upper sedimentary section, the seismic reflection pattern between meters 600 and 1000 differs from most of the remainder of the profile, with a thinner sequence of reflectors from the near surface to about 150 m depth (Appendix D). The thinner sequence of reflectors form a concave shaped pattern down to a depth of about 150 m. This pattern of reflectors is similar to that observed in the present Mojave River channel on Line 3 (see below), suggesting that the thinner sequence of reflectors may represent a buried river channel (paleo channel). The depth range of the possible paleo channel is consistent with that of the upper alluvial unit identified in boreholes in the region. The seismic data indicate that the possible paleo channel is fault bounded and that it overlies a structural depression in the underlying crystalline rocks. Layers outside of the possible paleo channel appear to continue within the channel at a structurally lower level. If this feature represents a paleo-river channel, then the lateral continuation of some layers beyond the channel's narrow confines suggests that the feature was not

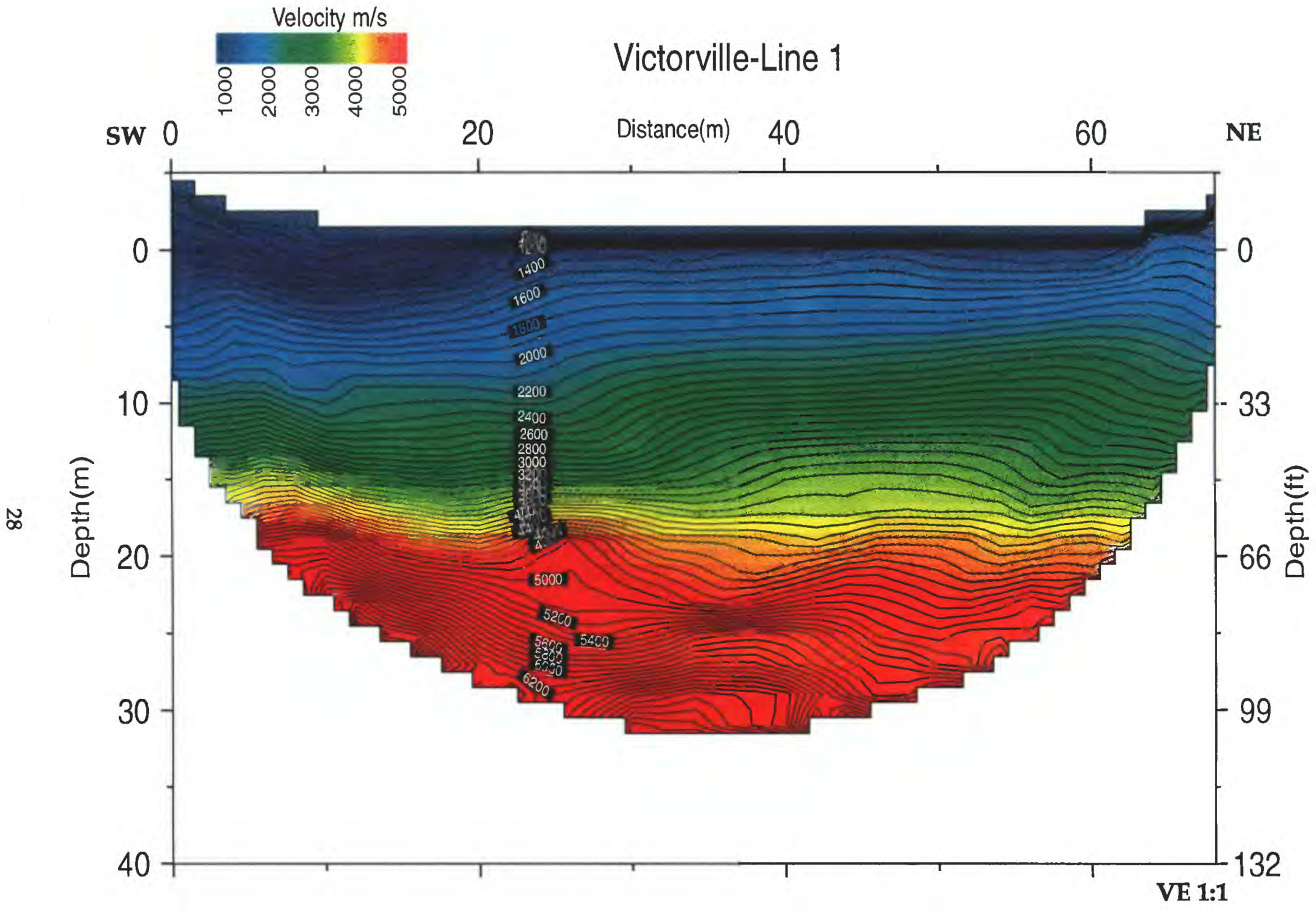

Fig. 18 Seismic velocity inversion model for Line 1. Velocities are in meters per second.

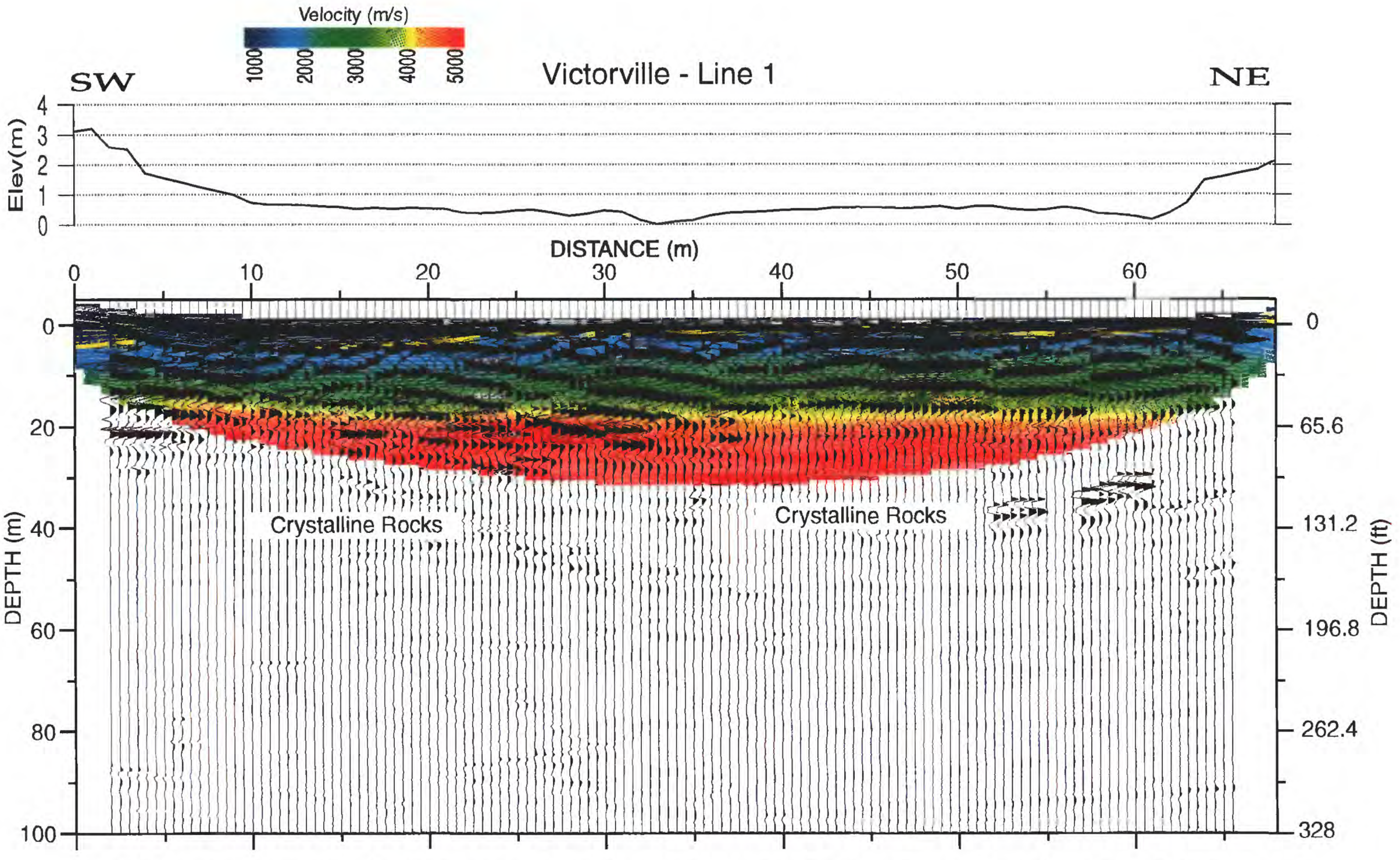

Fig. 19. Combined seismic reflection image and velocity model along Line 1. The yellow contour shows the 1500 m/s velocity contour (probable water level).

Processing Parameters
line 1r1 k1 a3 p3 v32: agc = 15, fk = 90-400, 1-600, 50%, bp = 200-400-800-1600
mig = 400, 30, 90 poststack: bp = 150-300-800-1600, agc = 500

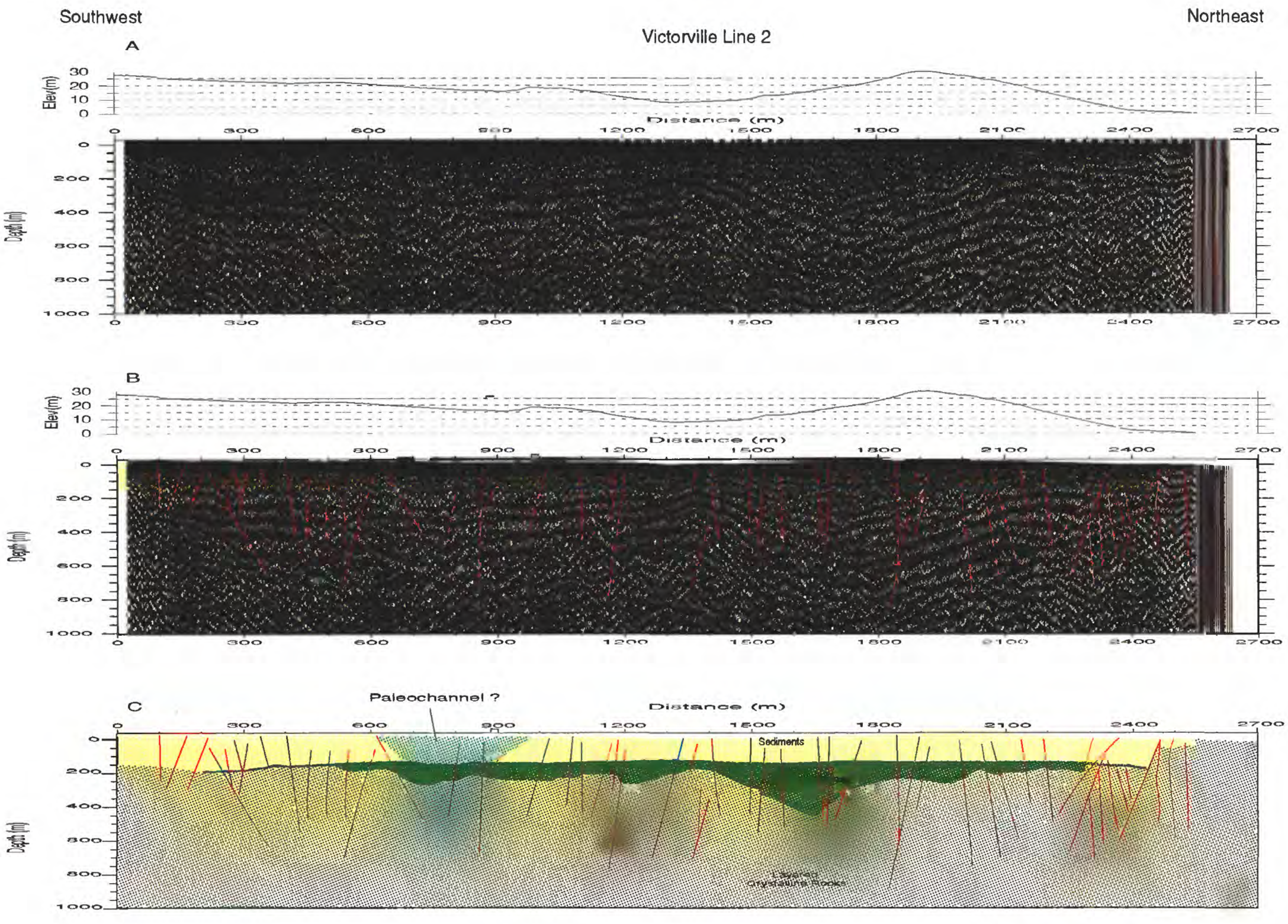

Fig. 20 (a) Seismic reflection image for Line 2. (b) Interpreted seismic reflection image for Line 2. The maximum thickness of the sedimentary (consolidated and unconsolidated) section is shown in yellow. The blue line marks the top of rocks with a velocities of 6 km/s or more. Red lines depict interpreted faults. (c) Interpreted section along Line 3. The yellow color depicts sediments. The grey area outlines a possible paleo-river channel. The green area is interpreted as massive crystalline rocks. The brown area is interpreted as layered crystalline rocks, such as limestone, marble, or quartzite.

incised into existing sediments or bedrock. Instead, some alluvial facies, presumably river channel deposits, may have persistently accumulated in shallow tectonic depression on a river floodplain that was continually renewed by syndepositional faulting.

From about 150 to about 200 m depth, the unmigrated seismic section shows fewer reflections and numerous diffractions, suggesting a significant change in subsurface materials. Although depth varies laterally, below about 200 m depth, there are a series of strong reflectors that appear to be faulted and folded. These reflectors are only about 75 m deep on the northeastern end of the profile, but rapidly deepen to over 100 m depth by meter 2400 of the seismic profile. In the distance range from about meter 2100 to about meter 1700, the reflections appear to dip to the southwest, and from about meter 1700 to about meter 1500, the reflections dip to the northeast, suggesting a series of folds across the profile. However, some of the reflections on the seismic section are probably diffracted energy that originate from layered rocks within the basement where it forms high points or is faulted. In general, there are topographic highs in the reflective basement from meters 2000 to 2700 and from meters 1300 to 1400. Basement appears to sharply deepen to the southwest between meters 400 and 0, suggesting a deeper basin to the southwest.

In the seismic reflection section, faults are inferred by vertical displacements of a sequence of reflections that are observed laterally over hundreds of meters or several kilometers. On unmigrated reflection sections, faulting is also inferred by numerous diffractions. Such faulting is apparent in several locations at depths ranging from the crystalline bedrock to the near surface along the entire length of Line 2. Two of the most prominent of these faults that reach the near surface are observed between meters 1310 and 1400. The deeper layered crystalline rocks also show evidence of faults, some of which continue to the near surface (Fig. 20b). The largest fault offset occurs near the northeastern end of the seismic profile near meter 2500 where crystalline basement apparently rises near the surface. However, other prominent faults and folds in crystalline basement are apparent throughout the seismic profile (Fig. 20c).

Interpreted Refraction Section

The seismic refraction data from Line 2 was inverted as described for Line 1, and velocities were determined from the near-surface to approximately 200 m over most of the seismic profile (Fig. 21). Velocities range from about 1000 m/s at the surface to about 6200 m/s at an average depth of about 200 m over most of the profile. As explained for Line 1, seismic velocities in excess of about 5000 m/s likely represent massive crystalline rocks, and those below about 1500 m/s likely represent unconsolidated sediments. Velocities ranging from 2000 m/s to about 4000 m/s probably represent more consolidated sediments and clays or fractured crystalline rocks. An abrupt rise in basement is indicated by higher velocities (>4500 m/s) at shallower depths (<75 m) near the northeastern end of the

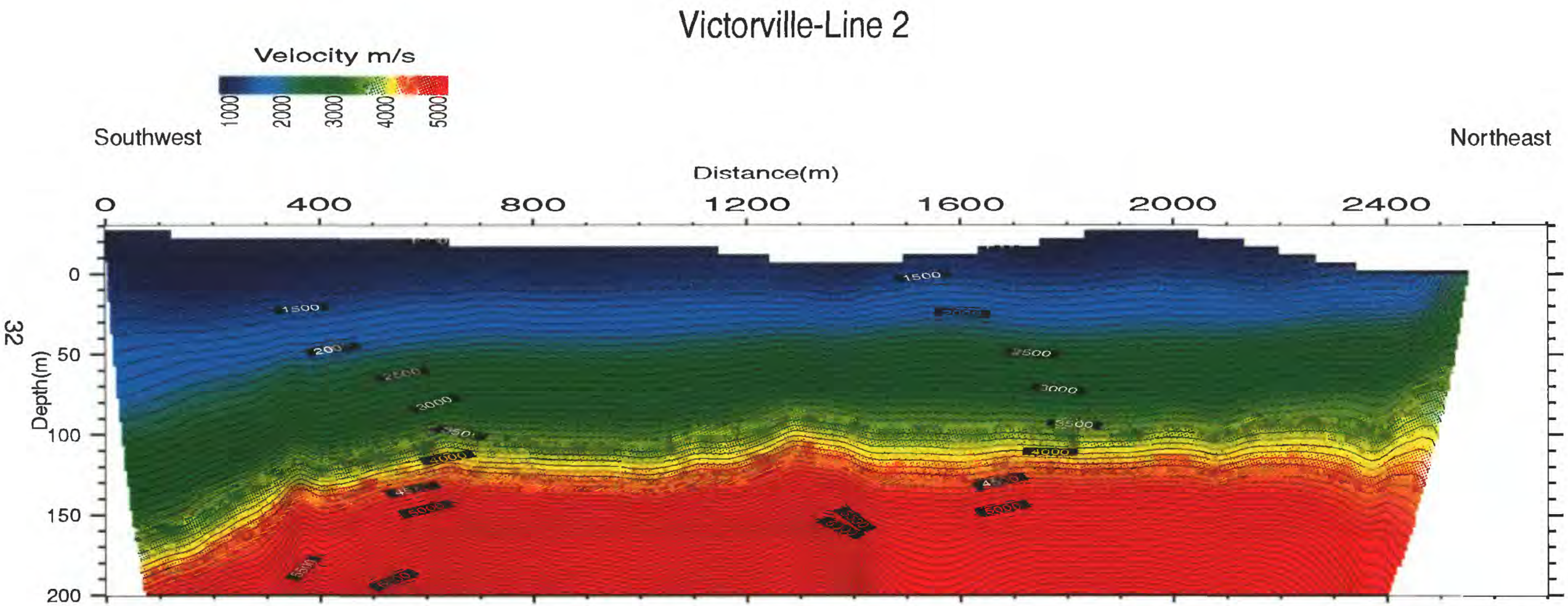

Fig. 21. Seismic velocity inversion model along Line 2. Velocities are in meters per second.

profile, and on the southwestern end of the profile, a southwesternly dipping basement is suggested by higher velocities (~4500 m/s) at greater depths (~200 m). Lateral variations in velocity correspond well to changes in the depth to bedrock (as inferred by the reflection image) and to other structural features along the seismic profile. In the area of the possible paleo-river channel described above, velocity contours are slightly deflected and structurally lower in the upper 50 m beneath the ground surface but show little lateral change at greater depths.

Combined Reflection and Refraction Sections

The seismic velocity image has been superimposed onto unmigrated and migrated reflection images along Line 2 (Figs. 22 and 23, respectively). The combined velocity and unmigrated reflection images show that the top of crystalline basement (>4500 m/s) is located at about 150 m depth along most of the profile. The top of crystalline basement, however, does not generate a single strong reflection, but instead, there are a series of diffractions (Fig. 22, Appendix D). The abundant refracted seismic energy suggests that the top of the crystalline rock is highly irregular or that there are numerous diffracting sources (such as boulders) at the sediment-basement contact. At about 200 m depth, however, the basement rocks appear to be well layered, and based on their velocities (>5000 m/s), they are probably crystalline.

Both the sedimentary section above 150 m depth and the crystalline rocks below appear to be highly faulted, as indicated by vertical offsets in reflectors along the profile. The layered crystalline rocks below the sediment-basement contact appear to be strongly folded into a series of anticlines and synclines that are inverted from the present-day topography (Fig. 22).

The seismic migration technique moves diffracted seismic energy, caused by faults and other point sources, to be placed in its proper position. The migrated image shown in Fig. 23 also has all frequencies below about 100 Hz removed, which helps to emphasize shallow reflectors in the upper 50 m and the sediment-basement interface. The top of crystalline basement at about 150 m depth is indicated by an increase in high-frequency reflective energy. The migrated, high-frequency signal differs from that along Line 1 (Fig. 17), where basement is nonreflective suggesting that the crystalline basement rocks beneath Line 2 are not massive and differ from those beneath Line 1. In the upper 100 m, a change in the reflection pattern between meters 600 and 1000 (see Figs. 22 and 23) occurs in the area of the interpreted paleo river channel discussed above.

On both seismic sections, the 1500 m/s coutour which is the approximate velocity of unconsolidated, saturated sediments (Schon, 1996) is highlighted in yellow (Figs. 22 and 23). The 1500 m/s velocity may indicate the static water level; if so, it suggests that the water level is near the surface in the vicinity of the Mojave River (near meter 2700) but may be about 60 m deep on the southwestern end of the profile. The greatest vertical variation in the 1500 m/s contour occurs near areas that show significant evidence of faulting. For example, near meter 1400, the 1500 m/s contour decreases by

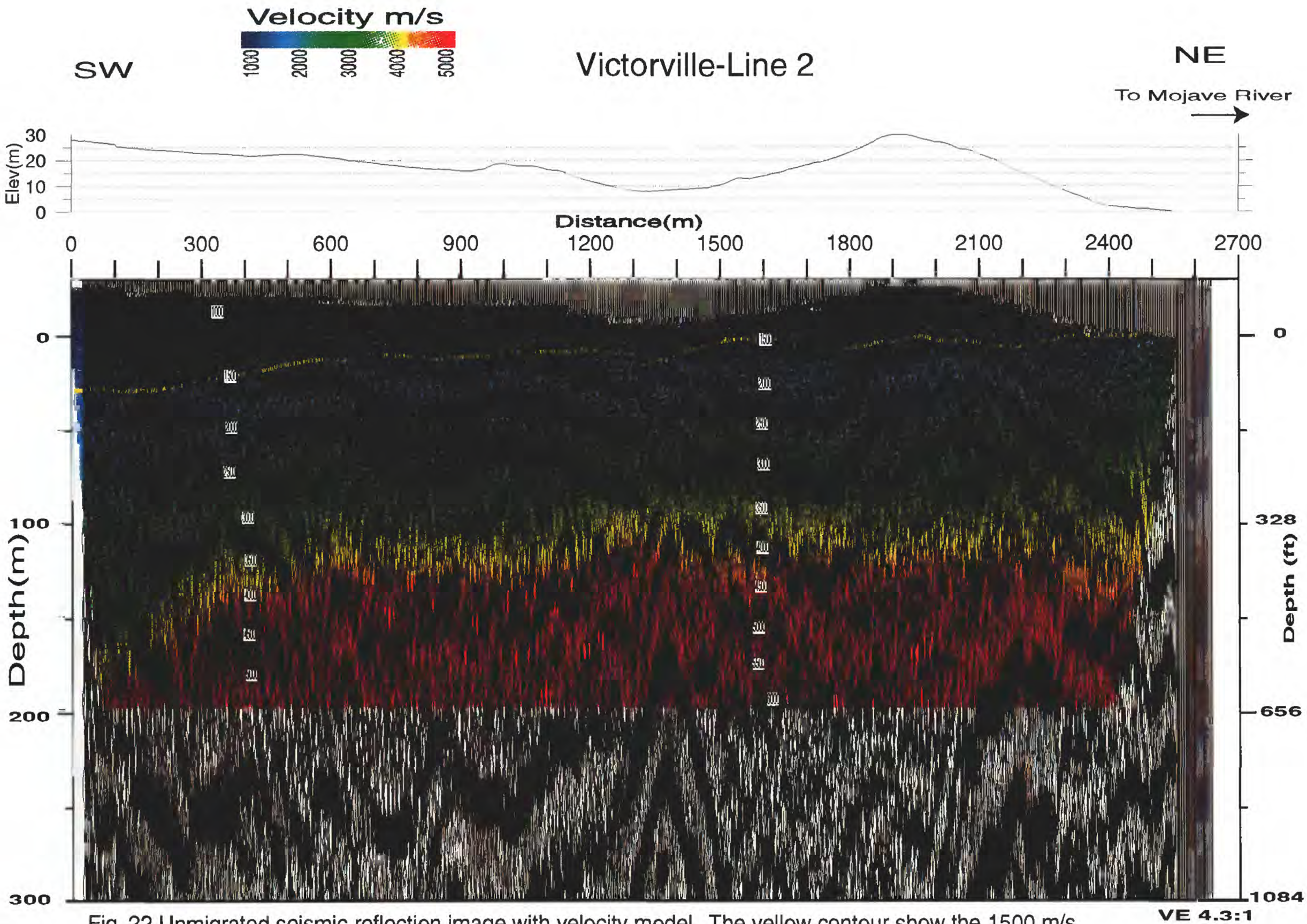

Fig. 22 Unmigrated seismic reflection image with velocity model. The yellow contour show the 1500 m/s contour (probable water level).

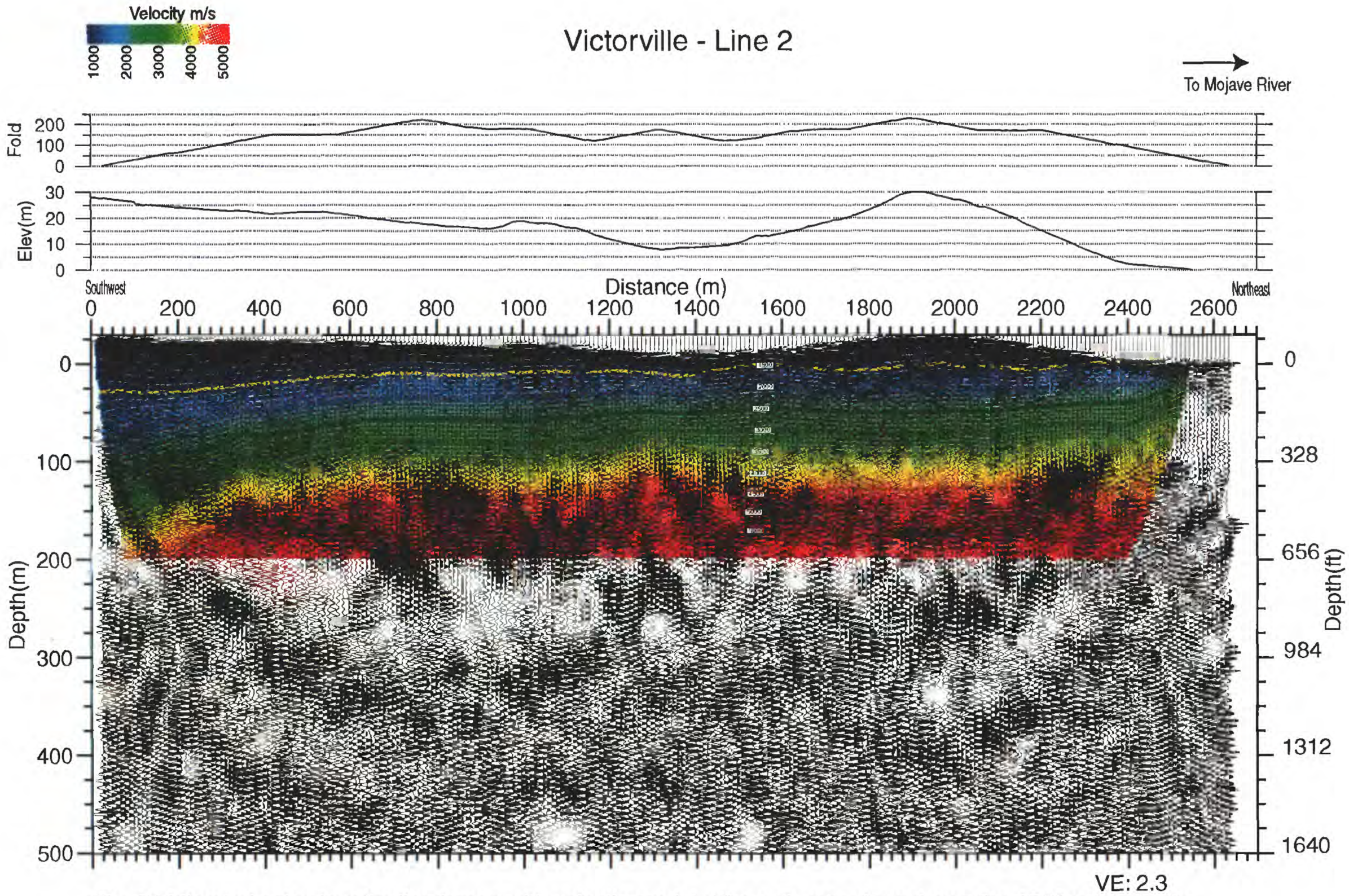

Fig. 23 Migrated seismic reflection image with velocity model. The yellow contour shows the 1500 m/s velocity contour (probable water level).

Processing Parameters
line 1r2 k1m1 a5 p4 v61: agc = 300, fk = 200-800, 1-800, 40%, bp = 20-40-600-1200, 60-4, 180-1
mig = 600, 500, 90 poststack: bp = 100-200-600-1200, agc = 200

about 15 m from the northeast to the southwest across faults (Fig. 22). Such a rapid drop in the water table across these faults would be expected if the faults act as barriers to water moving down from the topographic high at meter 1900. The 1500 m/s contour is largely planar at a depth of about 40 m across the possible paleochannel, but it dips southwestward across most of Line 2. Within the possible paleo channel, a planar, rather than a dipping water table would be expected due to planar layering within the overall concave shape of the channel.

Line 3

Interpreted Reflection Sections

Stacked, unmigrated seismic reflection images of the upper 200 m and 1000 m of Line 3 are shown in Figs. 24 and 25. Closeup views of this line are included in Appendix E. Low-frequency reflections, shown to be consistent with crystalline basement along Lines 1 and 2, are generated at average depths of about 50 m along Line 3, but there are clear highs and lows in basement along the profile. These basement highs and lows may be caused by faulting. Because the images shown in Figs. 24 and 25 are unmigrated, diffracted energy can obscure the true lateral variation in basement; thus, basement depths cannot be determined solely on the basis of the low-frequency, unmigrated reflections, especially on the northwestern end of the profile, where strong diffractions are observed.

Line 3 was located within or on the banks of the Mojave River, and thus, provides good images of reflectors within the river channel. Although they surely differ in age, the reflectors observed within the river channel are consistent in appearance with those observed within the apparent paleo channel from Line 2 (Fig. 22). If the sediments within the current river channel and those of the possible paleochannel were similarly deposited then the two channels are expected to have similar seismic signatures. As observed in the possible paleochannel of Line 2 (Fig. 20), thin, semi-continuous reflections are observed in the area of the current river channel on Line 3 (see meters 100 to 150 on Fig 24). However, the maximum depth differs, as the channel appears to be no greater than about 70 m deep along Line 3 and about 150 m deep along Line 2.

Vertical offsets in reflectors indicate that faulting occurs in about 4 separate zones along the profile, from about meters 0 to 200, at about meter 350, at about meter 475 , and about meter 950 distance (Fig. 20 c). Some of these faults may coincide with lineaments observed in granitic rocks on the north side of the Mojave River. Vertical offsets in the sediment-basement interface appear to be as much as 50 m and appear to occur along southeast-dipping faults. The central part of the seismic profile appears to form a horst, and from about meter 100 to meter 200, the data suggest that the crystalline basement forms a graben. From about meter 100 to meter 150, the seismic data suggest a deep concave-shaped channel extending from the surface to about 40 m depth, underlain by the apparent graben.

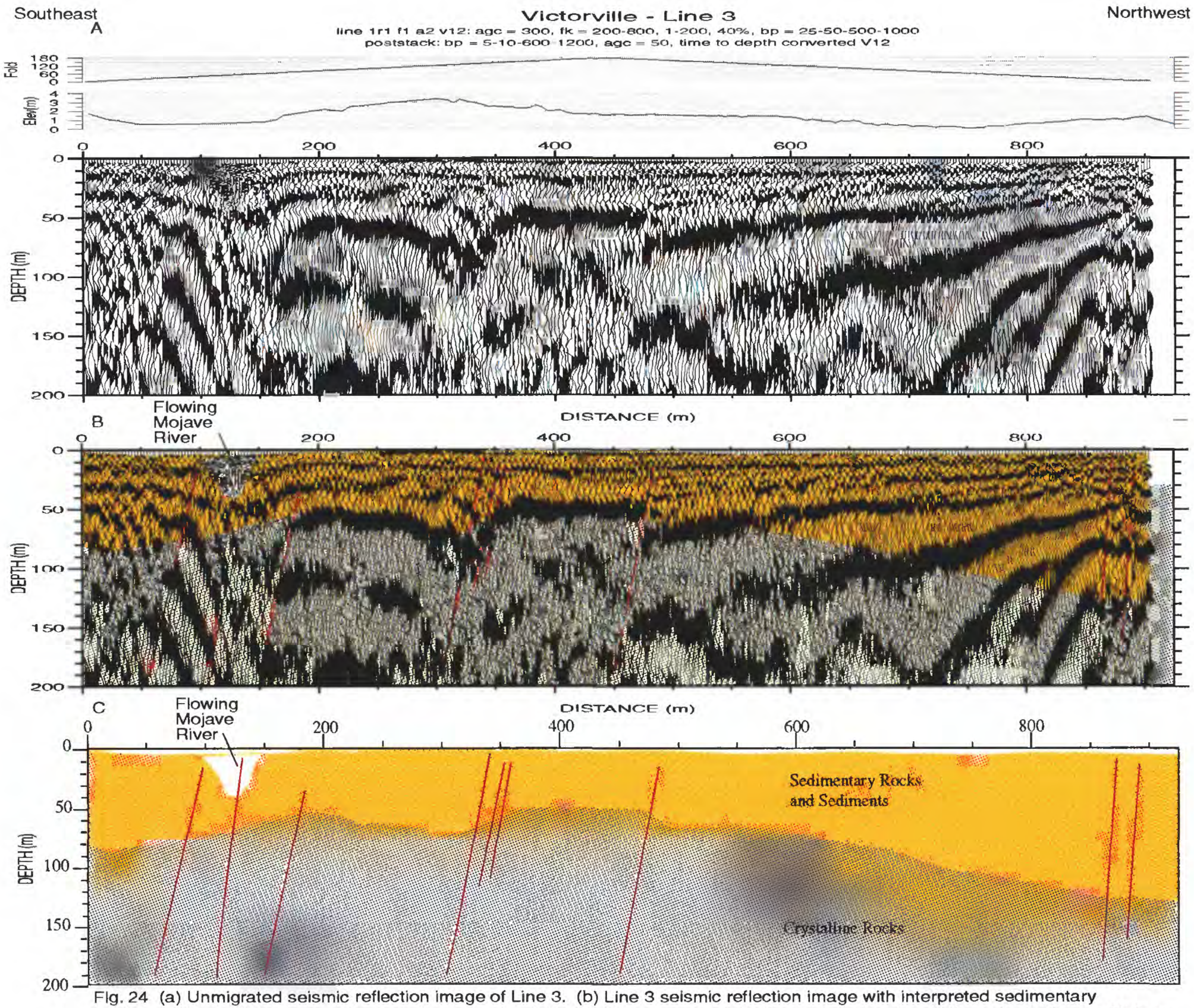

Fig. 24 (a) Unmigrated seismic reflection image of Line 3. (b) Line 3 seismic reflection image with interpreted sedimentary section (yellow). The uncolored area between meter 100 and 150 corresponds to the surface location of the actively flowing Mojave River. Red lines are interpreted faults. (c) Interpretative section along line 3.

Victorville - Line 3

Southeast

Northwest

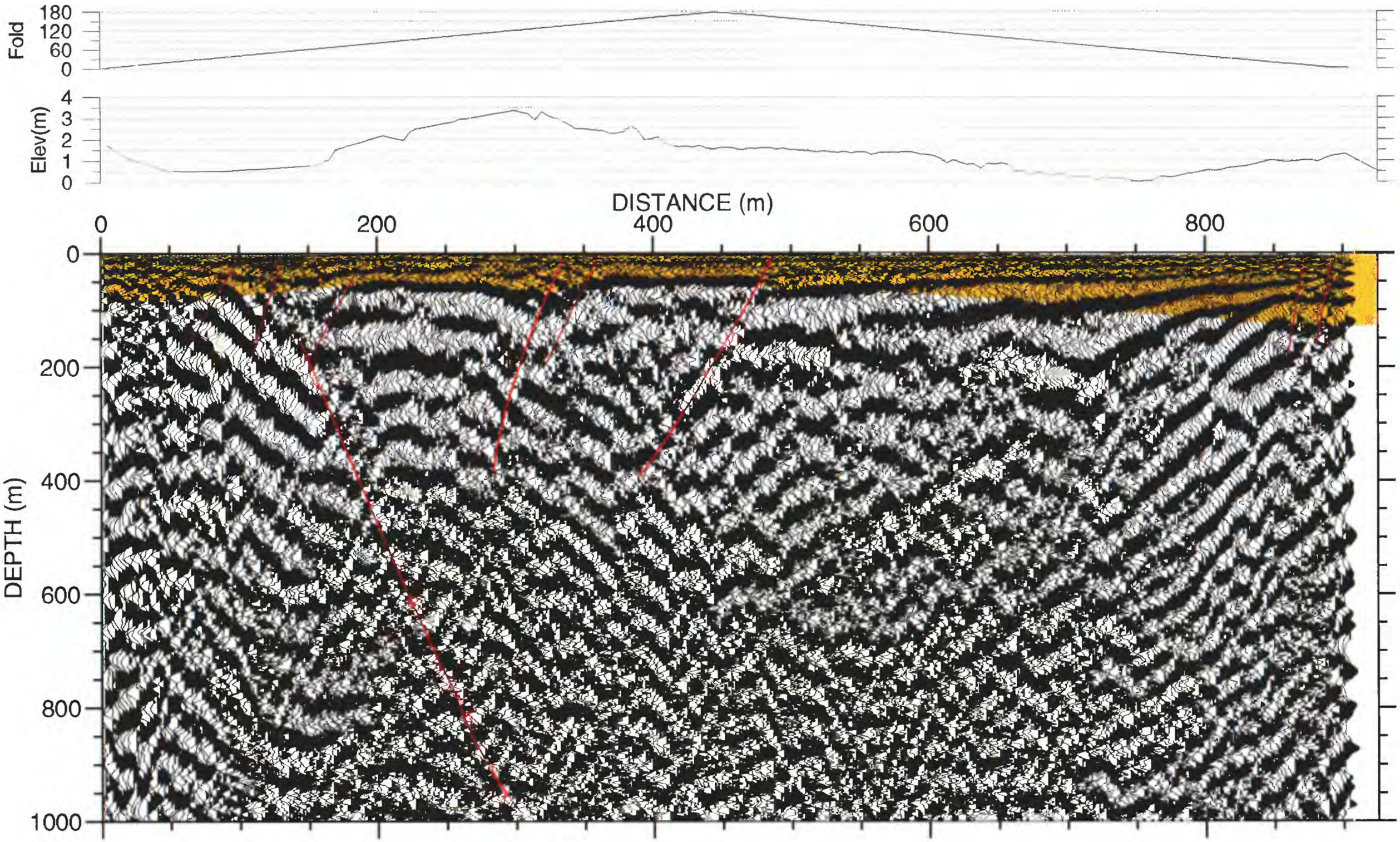

Fig. 25 Interpreted seismic section along line 3. Interpreted faults are shown in red and the sediments in yellow.

Processing Parameters
line 1r1 f1 a2 v12: agc = 300, fk = 200-800, 1-200, 40%, bp = 25-50-500-1000
poststack: bp = 5-10-600-1200, agcc = 50, time to depth converted V12

Interpreted Refraction Section

Velocities along Line 3 range from about 1000 m/s at the surface to about 6000 m/s at about 100 m depth (Fig. 26). Velocities consistent with sediments (<4000 m/s) are observed only within the upper 70 m along most of the seismic profile. This depth is consistent with our interpreted depth to crystalline basement based on the seismic reflection image. Seismic reflection images of the apparent basement horst and graben are consistent with vertical variations in the higher-velocity contours (>4500 m/s).

The seismic velocities are generally consistent with the reflection-images except on the northwestern end of the profile, where the reflection image suggests that bedrock decreases in depth. However,the apparent structural complexity on the northwestern end of the profile, as indicated by diffractions on the unmigrated seismic reflection image (Fig. 24), makes interpretation of the true structure difficult.

Combined Reflection and Refraction Sections

The velocity image has been superimposed on a migrated reflection image of Line 3 (Fig. 27). The high-frequency (>100 Hz), migrated reflection image shows strong reflected energy at depth ranges where the velocities are low (< 4000 m/s), but there are fewer coherent reflections corresponding to depths with higher velocities (>4000 m/s). These reflection and velocity patterns suggest that the higher-velocity rocks (basement) are probably not layered (Fig 28a). As along Line 1, the high-velocity, reflection-free section probably corresponds to crystalline basement (quartz-monzonite). Both the reflection and velocity images suggest that basement varies laterally in depth by about 50 m, with the horst and graben structure near the southeast crossing of the river. From about the center of the seismic profile (meter 400) to near the end of the profile, basement apparently dips to the northeast where it appears to be at least 100 m deep.

Seismic velocities over the apparent river channel between meters 100 and 150 increase to at least 1500 m/s at the surface, suggesting that the sediments are highly saturated within the river channel and along most of the profile. However, the 1500 m/s contour dips sharply to the northwest from about meter 550 to the northwest end of the profile. On the basis of the velocity contours, we suggest that saturated sediments may be as deep as 50 m on the northwestern end of the profile. The 1500 m/s contour (and presumably the water level) also appears to be as much as 30 m deep on the southeastern end of the profile, southeast of the active river channel (meter 0-50), and it appears to be as much as 10 m deep at meter 200, northwest and outside of the active river channel.

Summary and Conclusions

The seismic reflection and refraction profiles across the Mojave River at the Upper Narrows suggest that sediment thickness is no more than about 15-20 m thick at the Upper Narrows. Apparent offsets in reflectors suggest that the river channel occurs along faults that offset basement rocks (probably

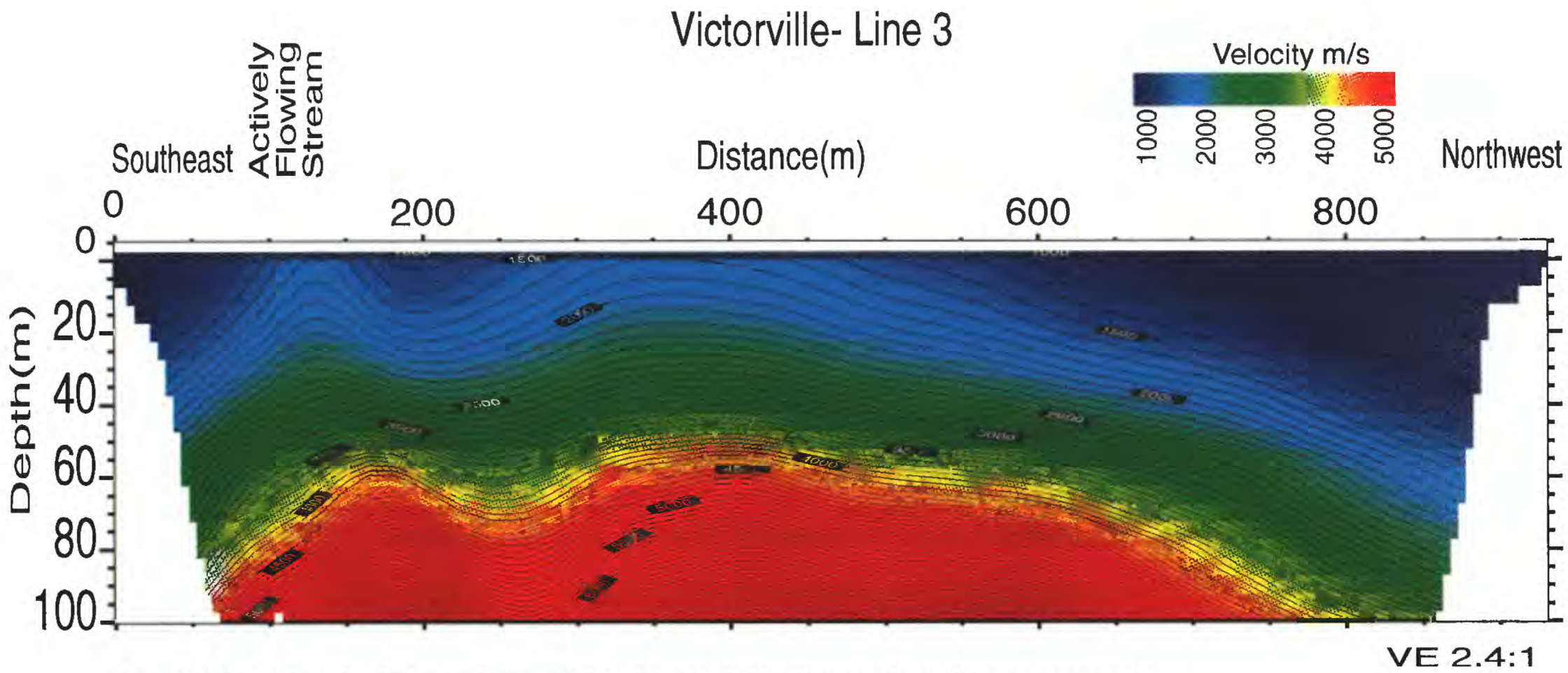

Fig. 26 Seismic velocity inversion model for Line 3. Velocities are in meters per second.

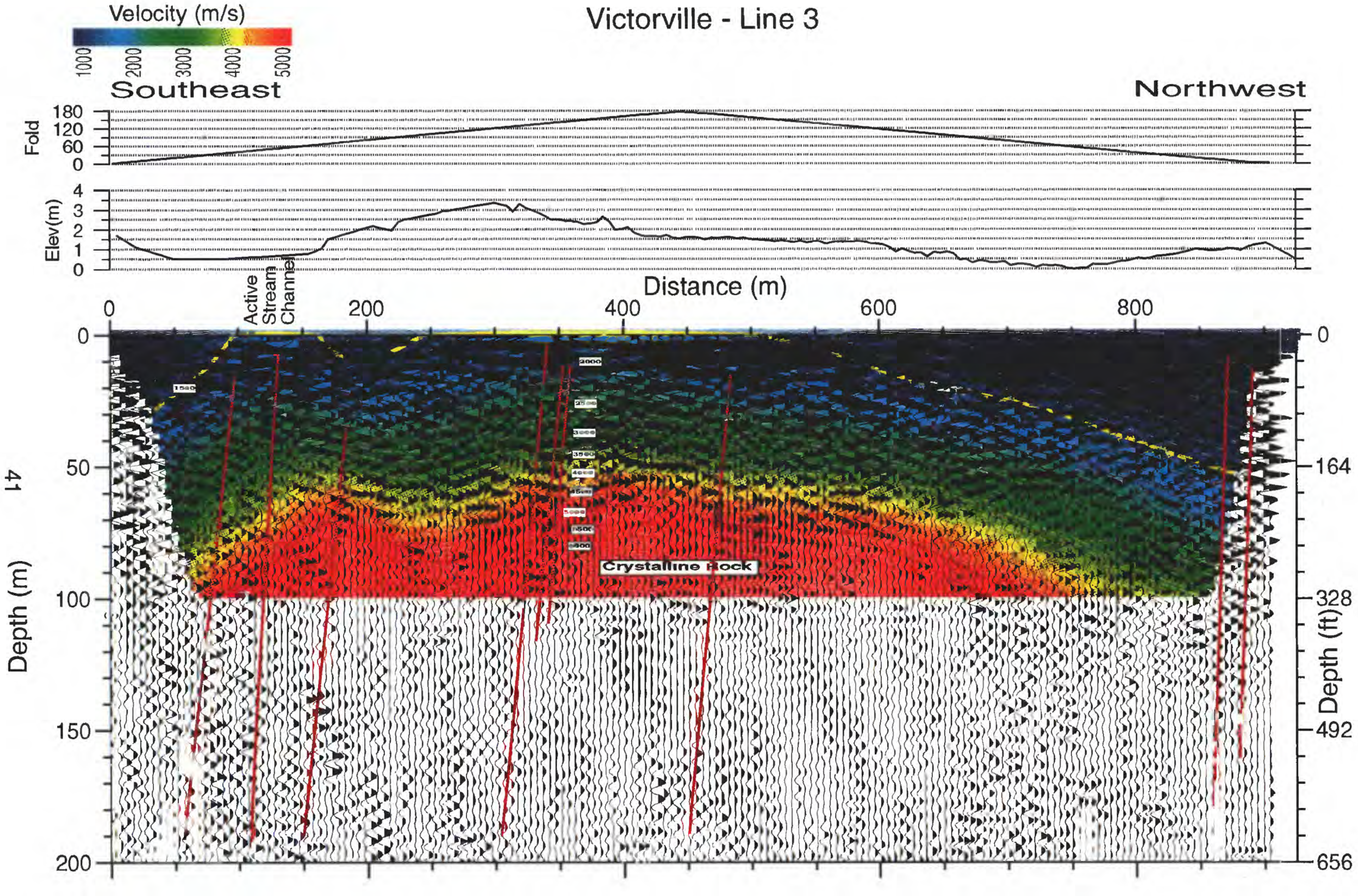

Fig. 27 Migrated seismic reflection image with the velocity model. Possible faults are shown as red lines. The yellow contour shows the 1500 m/s velocity contour (probable water level).

Processing Parameters
line 1r1 k1 a2 p1 v11: agc = 300, fk = 200-800, 1-200, 40%, bp = 25-50-500-1000, 60-3
mig = 200, 400, 90 poststack: bp = 100-200-1000-2000, agc = 500

Quartz Monzonite) and continue upward into the sediments of the river channel. Faulting along this segment of the Mojave River is not unexpected because the Victorville Fault trends near the seismic profile (see Fig. 1; Bowen, 1954). Velocities consistent with those expected for quartz monzonite (>5000 m/s) are observed at about 15 m depth across most of the profile. Both the reflection image and the velocity image are consistent with the depth to bedrock determined by Slichter (1905) at the Upper Narrows. The maximum volume of ground water flowing through the Upper Narrows at the crossing of Line 1 could be estimated on the basis of the depth to the 4000 m/s velocity contour (either clay or rock), assuming that the faults do not act as conduits to ground water flow.

Along Line 2, the velocity and reflection data indicate that the depth to crystalline basement rocks is no greater than about 150 m deep along most of the seismic profile but could be as little as 75 m on the NW end of the profile and about 200 m near the southwestern end of the profile. These results are consistent with previous gravity interpretations that imply a buried ridge of basement rocks underlying the area near Line 2 (Mabey, 1960; Subsurface Surveys, 1990). The seismic data indicate that basement rocks are displaced by a series of faults that have cumulatively offset crystalline rocks by as much as 100 m. Individual faults appear to have offset the crystalline rocks by several tens of meters in places, especially near the northeastern end of the profile. Some of the imaged faults geographically correspond to the locations of geologically mapped lineaments (Fig. 1b) that may extend for many kilometers to the south. It is likely that the faults affect groundwater flow in the region because faults in crystalline rocks have been shown to promote groundwater flow (Catchings et al., 1997; Jaasma et al., 1997), and in many cases faults in sediments are known to act as barriers to groundwater flow. Lateral variations in the depth to the 1500 m/s contour (probable water table) suggest that many of the faults act as barriers to groundwater flow within the sedimentary section. The 1500 m/s contours rises to the near-surface on the northeastern end of the profile, near the Mojave River but is as much as 60 m deep on the southwestern end of the profile. The seismic data are consistent with a buried paleo river channel along the profile, extending laterally from about meters 600 to 1000 and vertically from the near-surface to about 120 m depth. However, the seismic velocities below about 80 m may be too high to correspond to sediments that are unconsolidated enough to promote significant groundwater flow.

Along Line 3 at the Lower Narrows, sediment thicknesses are generally less than 70 m along the imaged profile, but near the ends of the profile, sediments may be more than 100 m thick. On the southeastern end of the profile, the seismic data suggest that the crystalline basement rocks form a horst and graben structure beneath the current channel of the Mojave River. On the northwestern end of the seismic profile, basement dips sharply to the northwest. The actively flowing near-surface channel of the Mojave River is imaged in the reflection sections as a sequence of thin reflectors, and the 1500 m/s contour (apparent water level) rises to the surface over the active

channel. The water level may dip sharply to the northwest near the end of the seismic profile, away from the active channel, and may be as much as 50 m deep there. Along most of the seismic profile, the 1500 m/s contour occurs within a meter of the surface. As similarly observed along Line 1 at the Upper Narrows, the river channel at the Lower Narrows appears to flow above an area of faulted basement rocks.

There appear to be significant vertical offsets in the underlying bedrock caused by faulting. Most faults observed on the seismic images can be traced from basement to the near-surface (within ~3 m in some places), possibly suggesting that there has been recent movement. The proximity of these faults to population centers of the Victor Valley and lifelines to greater southern California, combined with their shallow depth (suggesting young age) indicate that there is a considerable earthquake hazard. Seismic velocities are low enough (Vp = 1000 m/s) and sediment thicknesses are great enough (up to 200 m) to raise the concern of enhanced ground motions from earthquakes on local or regional faults (Borcherdt and Glassmoyer, 1994). Reflected seismic energy from movement on regional faults (Catchings and Kohler, 1996), combined with the presence of sedimentary basins, also raises the concern of significant ground motions that may be damaging to local facilities and to regional lifelines.

Although seismicity within the Victor Valley is not particularly high at present, large magnitude earthquakes have occurred nearby (Landers Earthquake in 1992 and Hector Mine Earthquake in 1999). Therefore, mitigating measures should be undertaken to protect lives and property in the Victor Valley and regional lifelines that serve the major Southern Californian metropolitan areas.

Data Availability

The data are available in SEG-Y format (with elevation and timing corrections applied) from the principal investigator, R.D. Catchings, at the address on the front of this report.

Acknowledgments

This investigation was undertaken at the request of and funded by the Mojave Water Agency and the U. S. Geological Survey's Water Resources Division. We wish to thank Mr. Norman Caouette and the Mojave Water Agency for assistance and funding. Field assistance was provided by Tom Burdette, Katharine Favret, Angie, Jose Rodriguez, Joe Grow, Andy Gallardo, Monique Welch, Shad Betham, Allen Yong, Tracy Pattelena, and Mark Shularen. Technical review by Deborah Underwood is greatly appreciated.

References

Armstrong, R.L., and Suppe, J., 1973, Potassium-Argon geochronometry of Mesozoic igneous rocks in Nevada, Utah, and southern California: Geological Society of America Bulletin, v. 84, p. 1375-1392.

Borcherdt, R. D. and G. Glassmoyer, 1994, Influences of local geology on strong and weak ground motions recorded in the San Francisco Bay region and their implications for site-specific building code provisions, in The Loma Prieta, California Earthquake of October 17, 1989- Strong Ground Motion, U. S. Geological Survey Professional Paper 1551-A, 77-109.

Bortungo, E.J., and T.E. Spittler, 1986, Geologic map of the San Bernardino Quadrangle, California, California Department of Mines and Geology, Regional Geologic Map Series, map No. 3A, sheet 1 of 5, Scale 1:250,000.

Bowen O.E. Jr., 1954, Geology and mineral deposits of the Barstow Quadrangle, San Bernardino County, California: California Division of Mines Bulletin 165, p. 1-185.

Catchings, R. D., and W. M Kohler, 1996, Reflected seismic waves and their effect on strong shaking during the 1989 Loma Prieta, CA Bull. Seismological Society of America, v. 86, p.1401-1416.

Catchings, R. D. and W.H.K. Lee, 1996, Shallow velocity structure and Poisson's ratio at the Tarzana, California strong-motion accelerometer site, Bull. Seismol. Soc. America, v. 86, p. 1704-1713.

Catchings, R. D., M. N. Jaasma, M. R. Goldman, and M. J. Rymer, 1997, Seismic images beneath the Continental (Bottomless Pits) area of Flagstaff, Arizona, US Geological Survey Open-file Report, 36 p.

Chrisley, S.M., 1997, Geology and hydrogeology of the George Air Force Base vicinity, California [M.S. thesis]: San Jose, California, San Jose State University, 111 p.

Christensen, N. I. (1996), Poisson's ratio and crustal seismology, J. Geophys. Res. 101, 3139-3156.

Cox, B.F., J.W. Hillhouse, A.M. Sarna-Wojcicki, and J.C. Tinsley, III, 1998, Pliocene-Pleistocene depositional history along the Mojave River north of Cajon Pass, California--regional tilting and drainage reversal during uplift of the central Transverse Ranges: Geological Society of America Abstracts with Programs, v. 30, no. 5, p. 11.

Cox, B.F., and J.C. Tinsley, III, 1999, Origin of the late Pliocene and Pleistocene Mojave River between Cajon Pass and Barstow, California, in Reynolds, R.E., and Reynolds, Jennifer, Tracks along the Mojave: A field guide from Cajon Pass to the Calico Mountains and Coyote Lake: San Bernardino County Museum Association Quarterly, v. 46, no. 3, p. 49-54.

Dibblee, T.W, 1960, Preliminary geologic map of the Victorville quadrangle: U.S. Geological Survey, Mineral Investigations Field Studies Map MF-229, scale 1:62,500.

_____, 1967, Areal Geology of the western Mojave Desert, California, U.S. Geological Survey Professional Paper 522, 153 p.

Dutcher, L.C., and G.F Worts, Jr., 1963, Geology, hydrology, and water supply of Edwards Air Force Base, Kern County, California: U.S. Geological Survey Open-File Report, 225 p.

Hole, J.A., 1992, Nonlinear high-resolution three-dimensional seismic travel time tomography, Journal Geophysical Research, 97, p. 6553-6562.

IT Corporation, 1992, Remedial Investigation, Operable Unit 2, Jp-4 spill, George Air Force Base, California, v. 1., San Bernardino, California.

Jaasma, M. N., R. D. Catchings, M. R. Goldman, and M. J. Rymer, 1997, Seismic images in the Skunk Canyon and Fox Glen areas of Flagstaff, Arizona, US Geological Survey Open-file Report, 49 p.

Jennings, C. W. 1977, Geologic Map of California, California Geologic Data Map Series, Map No. 2, 1:750,000.

Londquist, C.J., D.L. Rewis, D.L. Galloway, and W.F. McCaffrey, 1993, Hydrogeology and land subsidence, Edwards Air Force Base, Antelope Valley, California, January 1989-December 1991: U.S. Geological Survey Water-Resources Investigations Report 93-4114, 74 p.

Mabey, D.R., 1960, Gravity survey of the western Mojave Desert, California: U.S. Geological Survey Professional Paper 316-D, p. 51-73.

Mavko, G., T. Mukerji, and J. Dvorkin,1996, Rock Physics Handbook, Stanford Rock Physics Laboratory, Stanford University, Stanford, California, 323 pp.

Meisling, K.E., and R.J. Weldon, 1989, Late Cenozoic tectonics of the northwestern San Bernardino Mountains, southern California: Geological Society of America Bulletin, v. 101, p. 106-128.

Miller, E.L., 1981, Geology of the Victorville region, California: Geological Society of America Bulletin, Part II, v. 92, no. 4, p. 554-608.

Miller, E.L., and J.F. Sutter, 1981, 40Ar/39Ar age spectra for biotite and hornblende from plutonic rocks in the Victorville region, California: Geological Society of America Bulletin, Part I, v. 92, p. 164-169.

Miller, F.K., and D.M. Morton, 1980, Potassium-argon geochronology of the eastern Transverse Ranges and southern Mojave Desert, southern California: U.S. Geological Survey Professional Paper 1152, 30 p.

Montgomery Watson [geotechnical consultants], 1995, George Air Force Base Installation Restoration Program OU 1 pre-design study (draft report, July, 1995), Walnut Creek, California.

Nur, Amos, 1982, Stanford Rock Physics Progress Report, January 1982, v. 13, Stanford Junior University, Stanford, California, 121 p.

Radian Corporation (Radian), 1989, Hydrological Studies in Support of Jurisdictional Determination for Application No. 29163, George Air Force Base.

Schon, J. H., 1996, Physical Properties of Rocks: Fundamentals and Principals of Petrophysics, Handbook of Geophysical Exploration, Seismic Exploration Vol 18, Elsevier Science, Inc., Tarrytown, N. Y.

Sibbett, B.S., 1999, Pleistocene channels of the Mojave river near Victorville, California, in Reynolds, R.E., and Reynolds, Jennifer, Tracks along the Mojave: A field guide from Cajon Pass to the Calico Mountains and Coyote Lake: San Bernardino County Museum Association Quarterly, v. 46, no. 3, p. 65-68.

Slichter, C. S., 1905, Field measurements of the rate of movement of underground water: U. S. Geological Survey Water-Supply Paper, v. 140, 122p.

Stewart, J.H. and F.G. Poole, 1975, Extension of the Cordilleran miogeosynclinal belt to the San Andreas Fault, southern California: Geological Society of America Bulletin, v. 86, p. 205-212.

Subsurface Surveys, Inc., 1990, Inventory of ground water stored in the Mojave River basins: unpublished report, prepared for Mojave Water Agency, Apple Valley, California, 47 p.

Appendix A

Distances and elevations along seismic Line 1

Measurements are relative to the first shotpoint.

Shot Number	Shot Dist. (m)	Shot Elev. (m)	Geophone Dist	Geophone Elev. (m)
1	0	3.1		
2	1	3.19		
3	2	2.58		
4	3	2.51		
5	4	1.7	4	1.7
6	5	1.56	5	1.56
7	6	1.43	6	1.43
8	7	1.26	7	1.26
9	8	1.13	8	1.13
10	9	1	9	1
11	10	0.73	10	0.73
12	11	0.67	11	0.67
13	12	0.67	12	0.67
14	13	0.64	13	0.64
15	14	0.6	14	0.6
16	15	0.57	15	0.57
17	16	0.52	16	0.52
18	17	0.55	17	0.55
19	18	0.52	18	0.52
20	19	0.55	19	0.55
21	20	0.54	20	0.54
22	21	0.52	21	0.52
23	22	0.4	22	0.4
24	23	0.37	23	0.37
25	24	0.4	24	0.4
26	25	0.47	25	0.47
27	26	0.49	26	0.49
28	27	0.39	27	0.39
29	28	0.28	28	0.28
30	29	0.35	29	0.35
31	30	0.46	30	0.46
32	31	0.43	31	0.43
33	32	0.16	32	0.16
34	33	0	33	0
35	34	0.08	34	0.08
36	35	0.14	35	0.14
37	36	0.28	36	0.28
38	37	0.38	37	0.38
39	38	0.4	38	0.4
40	39	0.43	39	0.43
41	40	0.46	40	0.46

42	41	0.48	41	0.48
43	42	0.48	42	0.48
44	43	0.55	43	0.55
45	44	0.56	44	0.56
46	45	0.57	45	0.57
47	46	0.55	46	0.55
48	47	0.54	47	0.54
49	48	0.56	48	0.56
50	49	0.59	49	0.59
51	50	0.5	50	0.5
52	51	0.6	51	0.6
53	52	0.59	52	0.59
54	53	0.51	53	0.51
55	54	0.47	54	0.47
56	55	0.48	55	0.48
57	56	0.57	56	0.57
58	57	0.51	57	0.51
59	58	0.36	58	0.36
60	59	0.33	59	0.33
61	60	0.27	60	0.27
62	61	0.16	61	0.16
63	62	0.38	62	0.38
64	63	0.71	63	0.71
65	64	1.46		
66	65	1.58		
67	66	1.7		
68	67	1.82		
69	68	2.13		

Appendix B

Distances and elevations along seismic Line 2.
Measurements are relative to first shotpoint.

Shot Number	Shot Dist. (m)	Shot Elev. (m)	Geophone Dist	Geophone Elev. (m)
1	0	27.88		
2	4.84	27.84		
3	9.97	27.78		
4	14.89	27.69		
5	20	27.58		
6	24.97	27.55		
7	29.93	27.62		
8	34.93	27.49		
9	39.85	27.27		
10	44.8	27.28		
11	49.96	27.17	49.81	27.12
12	54.81	27.08	54.81	27.12
13	59.92	26.95	59.81	27.12
14	64.88	26.83	64.82	27.07
15	69.94	26.86	69.91	26.97
16	74.96	26.74	74.91	26.83
17	79.99	26.61	79.91	26.69
18	85.01	26.49	84.92	26.62
19	89.98	26.41	89.92	26.55
20	94.95	26.32	94.9	26.49
21	99.92	26.24	99.81	26.32
22	104.92	25.09	104.82	26.12
23	109.78	25.28	109.82	25.92
24	114.76	25.17	114.83	25.72
25	119.75	25.06	119.83	25.52
26	124.74	24.94	124.84	25.32
27	129.72	24.83	129.84	25.12
28	134.79	24.75	134.85	24.92
29	139.88	24.8	140	24.84
30	144.91	24.74	144.75	25
31	149.93	24.67	149.8	24.74
33	159.98	24.55	154.9	24.66
34	164.97	24.48	159.95	24.54
35	169.96	24.4	164.87	24.56
36	174.95	24.33	169.88	24.48
37	179.95	24.26	174.89	24.41
38	184.94	24.19	179.9	24.34
39	189.93	24.11	184.91	24.26
40	194.92	24.04	189.92	24.19
41	199.98	24.03	194.93	24.11
43	209.96	23.94	200.02	24.1

44	215.19	23.93	204.9	24.09
45	220.25	23.9	209.78	24.07
46	225.3	23.86	214.88	23.91
47	229.99	23.79	219.78	23.91
48	235.09	23.74	224.95	23.85
49	240.2	23.68	229.96	23.8
50	245.3	23.63	235.01	23.74
51	250.2	23.54	239.94	23.69
52	255.1	23.46	244.88	23.65
53	260	23.37	249.81	23.6
54	264.99	23.29	254.76	23.48
55	269.98	23.2	259.82	23.45
56	274.94	23.14	264.81	23.49
57	279.89	23.08	269.81	23.52
58	284.94	23.02	274.8	23.56
59	289.99	22.97	279.79	23.59
60	294.98	22.93	284.9	23.08
61	299.96	22.89	290	23.01
62	304.95	22.86	294.98	22.97
63	309.94	22.82	299.96	22.92
65	319.91	22.74	304.94	22.88
67	329.88	22.67	309.92	22.84
69	339.86	22.6	314.9	22.79
71	349.83	22.52	319.88	22.75
73	359.78	22.44	324.85	22.71
75	369.86	22.3	329.83	22.66
76	374.9	22.23	334.81	22.62
77	379.94	22.16	339.79	22.58
78	384.97	22.09	344.77	22.53
79	390	22.01	349.75	22.49
80	395.03	21.94	354.88	22.45
81	399.96	21.85	359.86	22.39
82	404.99	21.8	364.84	22.34
83	410.03	21.74	369.82	22.28
84	415	21.73	374.8	22.22
85	419.96	21.71	379.88	22.16
86	424.93	21.7	384.97	22.1
87	429.91	21.75	389.99	22.03
88	434.89	21.81	394.98	21.98
89	439.86	21.86	399.96	22.03
90	444.84	21.91	404.93	22.08
91	449.82	21.97	409.9	22.15
92	454.8	22.02	415.13	22.17
93	459.82	22.08	419.97	22.13
94	464.85	22.13	424.92	22.11
95	469.88	22.19	429.87	22.06

96	474.9	22.24	434.83	22.1
97	479.93	22.3	439.78	22.13
98	484.95	22.35	444.74	22.17
99	489.94	22.34	449.9	22.12
100	494.93	22.34	454.87	22.41
101	499.91	22.33	459.81	22.47
102	504.9	22.33	464.76	22.53
103	509.89	22.32	469.7	22.59
104	514.88	22.31	474.85	22.65
105	519.87	22.31	479.86	22.69
106	524.85	22.3	484.87	22.74
107	529.84	22.3	489.87	22.74
108	534.83	22.29	494.87	22.74
109	539.82	22.19	499.88	22.74
110	544.82	22.1	504.88	22.74
111	549.81	22	509.88	22.74
112	554.8	21.9	514.88	22.74
113	559.8	21.81	519.88	22.74
114	564.79	21.71	524.88	22.74
115	569.78	21.61	529.89	22.74
116	574.78	21.52	534.89	22.74
117	579.77	21.42	539.89	22.74
118	584.77	21.33	544.71	22.64
119	589.76	21.23	549.72	22.56
120	594.75	21.13	554.72	22.45
121	599.75	21.04	559.73	22.35
122	604.74	20.94	564.73	22.24
123	609.73	20.84	569.74	22.14
124	614.73	20.75	574.74	22.03
125	619.72	20.65	579.75	21.93
126	624.82	20.46	584.75	21.82
127	629.89	20.31	589.76	21.72
128	634.97	20.16	594.76	21.61
129	639.77	20.04	599.77	21.51
130	644.78	19.95	604.77	21.4
131	649.8	19.86	609.74	21.21
132	654.81	19.76	614.71	21.01
133	659.83	19.67	619.68	20.82
134	664.84	19.58	624.61	20.78
135	669.8	19.47	629.73	20.65
136	674.75	19.48	634.72	20.48
137	679.72	19.35	639.75	20.36
138	684.78	19.23	644.63	20.26
139	689.81	19.09	649.66	20.11
140	694.77	19.01	654.69	19.97
141	699.74	18.89	659.73	19.91

142	704.76	18.79	664.76	19.86
143	709.7	18.66	669.9	19.85
144	714.73	18.54	674.74	19.79
145	719.81	18.5	679.68	19.78
146	724.74	18.4	684.72	19.61
147	729.73	18.3	689.8	19.46
148	734.73	18.21	694.65	19.32
149	739.72	18.12	699.72	19.22
150	744.71	18.02	704.78	19.14
151	749.78	17.97	709.73	18.98
152	754.71	17.88	714.72	18.85
153	759.69	17.76	719.72	18.69
154	764.65	17.67	724.73	18.72
155	769.61	17.57	729.84	18.56
156	774.57	17.48	734.81	18.49
157	779.53	17.38	739.77	18.43
158	784.49	17.29	744.74	18.36
159	789.66	17.28	749.81	18.27
160	794.66	17.2	754.69	18.07
161	799.62	17.1	759.57	17.86
162	804.66	16.95	764.69	18.03
163	809.69	16.82	769.64	17.88
164	814.74	16.77	774.68	17.79
165	819.69	16.72	779.72	17.71
166	824.79	16.65	784.76	17.62
167	829.76	16.61	789.8	17.54
168	834.73	16.58	794.84	17.45
169	839.71	16.55	799.88	17.37
170	844.68	16.51	804.92	17.28
171	849.65	16.48	809.66	17.18
172	854.62	16.44	814.62	17.14
173	859.6	16.41	819.61	17.09
174	864.57	16.37	824.6	17.04
175	869.57	16.31	829.58	16.99
176	874.57	16.25	834.57	16.94
177	879.57	16.19	839.61	16.9
178	884.56	16.13	844.65	16.85
179	889.56	16.07	849.69	16.81
180	894.56	16.01	854.6	16.74
181	899.56	15.91	859.51	16.68
182	904.56	15.82	864.52	16.65
183	909.54	15.83	869.71	16.59
184	914.52	15.84	874.63	16.58
185	919.51	15.85	879.64	16.51
186	924.49	15.86	884.65	16.43
187	929.54	16.01	889.65	16.39

188	934.51	16.14	894.52	16.3
189	939.53	16.29	899.56	16.24
190	944.6	16.36	904.49	16.12
191	949.73	16.55	909.54	16.08
192	954.53	16.71	914.41	16.12
193	959.52	17.09	919.33	16.07
194	964.51	17.46	924.49	16.24
195	969.5	17.84	929.56	16.42
196	974.49	18.22	934.54	16.59
197	979.49	18.55	939.56	16.7
198	984.49	18.58	944.53	16.57
199	989.5	18.6	949.75	16.75
200	994.51	18.63	954.7	16.88
201	999.51	18.66	959.55	17.29
202	1004.52	18.51	964.4	17.7
203	1009.51	18.39	969.45	18.23
205	1019.5	18.07	974.46	18.53
206	1024.57	17.96	979.52	18.7
207	1029.48	17.88	984.43	18.77
208	1034.43	17.81	989.47	18.8
209	1039.44	17.77	994.5	18.84
210	1044.58	17.81	999.54	18.87
211	1049.48	17.83	1004.45	18.8
212	1054.46	17.85	1009.49	18.71
213	1059.44	17.88	1014.44	18.58
214	1064.46	17.85	1019.54	18.41
215	1069.49	17.62	1024.4	18.21
216	1074.52	17.58	1029.41	18.01
217	1079.55	17.3	1034.48	17.78
218	1084.59	17.08	1039.52	17.9
219	1089.52	16.83	1044.57	18.02
220	1094.44	16.6	1049.46	18.07
221	1099.44	16.35	1054.47	18.13
222	1104.44	16.21	1059.45	18.09
223	1109.44	16.11	1064.38	18.08
224	1114.46	16.07	1069.44	17.89
225	1119.45	16	1074.46	17.71
226	1124.45	15.93	1079.45	17.49
227	1129.47	15.77	1084.45	17.27
228	1134.45	15.53	1089.44	17.05
229	1139.43	15.28	1094.44	16.82
230	1144.42	15.03	1099.43	16.6
231	1149.41	14.69	1104.43	16.38
232	1154.4	14.23	1109.42	16.16
233	1159.4	13.83	1114.45	16.14
234	1164.39	13.53	1119.4	16.08

235	1169.39	13.24	1124.39	16.01
236	1174.38	12.94	1129.38	15.95
237	1179.25	12.63	1134.38	15.66
238	1184.25	12.42	1139.37	15.38
239	1189.26	12.2	1144.29	15.06
240	1194.26	11.99	1149.33	14.67
241	1199.26	11.77	1154.36	14.29
242	1204.27	11.56	1159.4	13.9
243	1209.27	11.34	1164.37	13.61
244	1214.27	11.15	1169.35	13.31
245	1219.27	10.95	1174.32	13.02
246	1224.27	10.76	1179.35	12.69
247	1229.26	10.56	1184.33	12.34
248	1234.26	10.37	1189.3	12.04
249	1239.26	10.18	1194.18	11.88
250	1244.26	9.98	1199.22	11.68
251	1249.26	9.79	1204.26	11.49
252	1254.26	9.59	1209.29	11.29
253	1259.26	9.4	1214.33	11.09
254	1264.26	9.21	1219.29	10.89
255	1269.25	9.01	1224.34	10.68
256	1274.25	8.82	1229.3	10.49
257	1279.25	8.62	1234.26	10.29
258	1284.25	8.43	1239.23	10.07
259	1289.25	8.33	1244.2	9.86
260	1294.25	8.23	1249.2	9.68
261	1299.25	8.13	1254.21	9.49
262	1304.24	8.02	1259.21	9.31
263	1309.24	7.92	1264.21	9.12
264	1314.24	7.82	1269.21	8.94
265	1319.24	7.72	1274.22	8.75
266	1324.18	7.7	1279.22	8.57
267	1329.06	7.77	1284.2	8.43
268	1334.06	7.83	1289.18	8.3
269	1339.06	7.88	1294.2	8.2
270	1344.06	7.94	1299.2	8.12
271	1349.06	7.99	1304.28	8.01
272	1354.06	8.05	1309.25	7.93
273	1359.06	8.11	1314.22	7.86
274	1364.06	8.16	1319.19	7.78
275	1369.06	8.22	1324.23	7.76
276	1374.06	8.28	1329.19	7.81
277	1379.06	8.33	1334.19	7.74
278	1384.06	8.39	1339.21	7.64
279	1389.06	8.44	1344.18	7.61
280	1394.06	8.5	1349.21	7.58

281	1399.06	8.56	1354.24	7.5
282	1404.05	8.61	1359.22	7.43
283	1409.05	8.67	1364.2	7.37
284	1414.05	8.73	1369.18	7.32
285	1419.05	8.78	1374.16	7.27
286	1424.05	8.84	1379.14	7.22
287	1429.05	8.89	1384.13	7.18
288	1434.05	8.95	1389.11	7.13
289	1439.05	9.01	1394.09	7.08
290	1444.05	9.06	1399.07	7.03
291	1449.05	9.12	1404.07	7.26
292	1454.05	9.18	1409.08	7.5
293	1459.05	9.23	1414.08	7.73
294	1464.05	9.29	1419.09	7.96
295	1469.05	9.34	1424.11	8.15
296	1474.05	9.4	1429.07	8.28
297	1479.06	9.57	1434.12	8.36
298	1484.07	9.75	1439.07	8.47
299	1489.08	9.92	1444.15	8.57
300	1494.09	10.09	1449.13	8.73
301	1499.1	10.27	1454.03	8.83
302	1504.11	10.44	1459.1	8.99
303	1509.12	10.82	1464.04	9.12
304	1514.07	11.2	1469.12	9.25
305	1519.02	11.57	1474.11	9.41
306	1523.97	11.95	1479.12	9.58
307	1528.91	12.33	1484.06	9.71
308	1533.86	12.7	1489.03	9.83
309	1538.81	13.08	1494.1	10
310	1543.83	13.02	1499.12	10.14
311	1548.85	12.96	1504.13	10.45
312	1553.88	12.9	1509.11	10.82
313	1558.9	12.85	1514.06	11.36
314	1563.92	12.79	1519.05	11.92
315	1568.94	12.73	1523.99	12.46
316	1573.94	12.92	1528.97	12.85
317	1578.94	13.11	1534.02	13.07
318	1583.93	13.3	1538.96	13.03
319	1588.93	13.48	1543.9	13
320	1593.93	13.67	1548.92	12.97
321	1598.93	13.86	1553.95	12.95
322	1603.93	14.05	1558.91	12.95
323	1608.92	14.24	1563.92	12.91
324	1613.92	14.43	1568.94	12.87
325	1618.92	14.62	1573.91	12.97
326	1623.92	14.81	1578.92	13.06

327	1628.92	14.99	1583.87	13.16
328	1633.91	15.18	1588.86	13.28
329	1638.91	15.37	1593.89	13.48
330	1643.91	15.56	1598.91	13.65
331	1648.77	15.85	1603.82	13.86
332	1653.8	16.2	1608.85	14.07
333	1658.87	16.46	1613.88	14.26
334	1663.83	16.67	1618.9	14.45
335	1668.81	16.83	1623.93	14.64
336	1673.9	17.03	1628.83	14.84
337	1678.79	17.23	1633.85	15.1
338	1683.82	17.51	1638.78	15.37
339	1688.8	17.73	1643.78	15.63
340	1693.78	17.94	1648.78	15.91
341	1698.76	18.15	1653.78	16.24
342	1703.74	18.37	1658.89	16.52
343	1708.72	18.58	1663.76	16.75
344	1713.7	18.8	1668.84	16.93
345	1718.7	18.94	1673.73	17.12
346	1723.82	19.11	1678.73	17.3
347	1728.74	19.19	1683.75	17.55
348	1733.73	19.33	1688.75	17.81
349	1738.71	19.56	1693.71	18.1
350	1743.68	19.8	1698.73	18.34
351	1748.66	20.03	1703.77	18.56
352	1753.63	20.27	1708.65	18.71
353	1758.61	20.5	1713.64	18.95
354	1763.74	20.79	1718.67	19.04
355	1768.71	21.02	1723.67	19.24
356	1773.72	21.36	1728.73	19.37
357	1778.63	21.64	1733.7	19.55
358	1783.63	21.96	1738.76	19.72
359	1788.63	22.28	1743.69	19.89
360	1793.65	22.64	1748.67	20.17
361	1798.59	22.93	1753.72	20.4
362	1803.58	23.32	1758.7	20.6
363	1808.6	23.62	1763.65	20.87
364	1813.49	23.98	1768.63	21.14
365	1818.52	24.28	1773.67	21.53
366	1823.5	24.69	1778.58	21.82
367	1828.51	24.98	1783.61	22.17
368	1833.53	25.42	1788.6	22.51
369	1838.61	25.76	1793.59	22.88
370	1843.58	26.15	1798.51	23.19
371	1848.44	26.6	1803.51	23.58
372	1853.57	27.01	1808.53	23.95

373	1858.48	27.44	1813.51	24.27
374	1863.4	27.94	1818.5	24.58
375	1868.35	28.33	1823.45	24.95
376	1873.33	28.77	1828.41	25.28
377	1878.43	29.01	1833.44	25.7
378	1883.51	29.38	1838.45	26.03
379	1888.22	29.48	1843.44	26.42
380	1893.31	29.62	1848.38	26.86
381	1898.4	29.77	1853.46	27.31
382	1903.38	29.89	1858.35	27.74
383	1908.35	29.88	1863.4	28.22
384	1913.32	29.89	1868.37	28.48
385	1918.26	29.9	1873.27	28.93
386	1923.31	29.87	1878.31	29.31
387	1928.27	29.75	1883.15	29.59
388	1933.08	29.77	1888.33	29.77
389	1938.28	29.55	1893.32	29.88
390	1943.32	29.52	1898.26	29.77
391	1948.29	29.17	1903.36	29.86
392	1953.35	28.95	1908.44	30.17
393	1958.26	28.69	1913.25	30.24
394	1963.28	28.43	1918.4	30.21
395	1968.23	28.17	1923.29	30.16
396	1973.33	27.98	1928.25	30.07
397	1978.28	27.77	1933.15	29.92
398	1983.19	27.67	1938.31	29.79
399	1988.19	27.46	1943.19	29.66
400	1993.18	27.24	1948.2	29.37
401	1998.18	27.03	1953.35	28.92
402	2003.07	26.93	1958.24	28.71
403	2008.18	26.97	1963.26	28.56
404	2013.24	26.82	1968.27	28.42
405	2018.25	26.67	1973.22	28.14
407	2028.22	26.24	1978.32	27.54
408	2033.1	25.9	1983.17	27.76
409	2038.09	25.66	1988.08	27.69
410	2043.22	25.01	1993.1	27.58
411	2048.04	24.72	1998.08	27.23
412	2053.11	24.4	2003.06	26.88
413	2058.06	24.12	2008.38	26.84
414	2063.1	24.16	2013.31	26.95
415	2068.09	24.11	2018.36	26.75
416	2073.16	24.06	2023.15	26.4
417	2078.03	23.65	2028.13	26.21
418	2083.02	23.42	2033.09	26.04
419	2088	23.09	2038.12	25.84

420	2093.08	22.87	2042.88	25.53
421	2098.06	22.42	2047.94	25.36
422	2103.08	22.08	2052.96	25
423	2108.02	21.79	2058.04	24.27
424	2112.95	21.46	2063.03	24.09
425	2117.87	21.12	2068.11	24.28
426	2122.91	20.88	2072.98	24.14
427	2127.94	20.56	2078.01	23.93
428	2132.99	20.3	2083.05	23.7
429	2137.84	19.96	2088.05	23.37
430	2142.9	19.63	2093.14	23.05
431	2147.91	19.16	2098.08	22.69
432	2152.92	18.73	2102.95	22.37
433	2157.8	18.23	2107.93	21.79
434	2162.75	17.82	2112.86	21.53
435	2167.8	17.37	2117.76	21.37
436	2172.66	16.88	2122.81	21.12
437	2177.66	16.48	2127.77	20.91
438	2182.68	16.14	2132.86	20.63
439	2187.59	15.79	2137.89	20.3
440	2192.69	15.41	2142.76	19.98
441	2197.69	15.07	2147.86	19.45
442	2202.68	14.75	2152.77	19.04
443	2207.65	14.42	2157.76	18.47
444	2212.65	14.05	2162.69	18.08
445	2217.63	13.72	2167.71	17.5
446	2222.68	13.36	2172.58	16.96
447	2227.6	13.01	2177.57	16.37
448	2232.6	12.66	2182.59	16.14
449	2237.56	12.32	2187.53	15.82
450	2242.57	11.99	2192.59	15.62
451	2247.53	11.64	2197.53	15.27
452	2252.59	11.29	2202.62	14.96
453	2257.51	10.94	2207.54	14.66
454	2262.57	10.65	2212.54	14.3
455	2267.46	10.25	2217.51	13.94
456	2272.51	9.94	2222.6	13.58
457	2277.48	9.59	2227.51	13.26
458	2282.63	9.23	2232.53	12.92
459	2287.47	8.9	2237.54	12.55
460	2292.54	8.56	2242.5	12.17
461	2297.41	8.22	2247.4	11.85
462	2302.41	7.89	2252.49	11.48
463	2307.4	7.55	2257.38	11.07
464	2312.4	7.2	2262.45	10.72
465	2317.32	6.9	2267.52	10.35

466	2322.47	6.54	2272.35	10.06
467	2327.37	6.25	2277.38	9.74
468	2332.3	5.92	2282.33	9.4
469	2337.27	5.6	2287.31	9.07
470	2342.44	5.33	2292.4	8.73
471	2347.29	4.96	2297.34	8.38
472	2352.39	4.59	2302.4	8.05
473	2357.27	4.32	2307.38	7.69
474	2362.28	3.98	2312.36	7.42
475	2367.21	3.72	2317.36	7.09
476	2372.39	3.38	2322.33	6.76
477	2377.19	3.06	2327.42	6.3
478	2382.3	2.81	2332.39	6.06
479	2387.07	2.6	2337.28	5.75
480	2392.24	2.37	2342.38	5.51
481	2397.23	2.18	2347.32	5.13
482	2402.16	2.04	2352.33	4.75
483	2407.28	1.94	2357.31	4.47
484	2412.39	1.83	2362.18	4.16
485	2417.15	1.76	2367.18	3.83
486	2422.23	1.68	2372.12	3.4
487	2427.25	1.55	2377.18	3.22
488	2432.44	1.5	2382.23	3.03
489	2437.16	1.47	2387.21	2.8
490	2442.17	1.42	2392.14	2.52
491	2447.13	1.37	2397.1	2.21
492	2452.38	1.19	2401.98	2.08
493	2457.16	1.17	2407.12	1.97
494	2462.07	1.06	2412.12	1.87
495	2467.24	1.03	2417.03	1.8
496	2472.23	1.03	2422.16	1.7
500	2492.17	1.05	2427.16	1.62
501	2497.11	0.89	2432.3	1.53
502	2502.13	0.81	2437.18	1.49
503	2507.14	0.72	2442.2	1.43
504	2512.15	0.64	2447.21	1.36
505	2517.17	0.56	2452.23	1.3
506	2522.21	0.52	2457.44	1.16
507	2527.15	0.47	2462	1.06
508	2532.2	0.41	2467.25	1.05
509	2537.09	0.34	2472.24	0.98
510	2542.01	0.16	2477.24	0.92
511	2547.18	0	2482.23	0.85
			2487.23	0.79
			2492.22	0.72
			2497.22	0.66

	2502.21	0.59
	2507.2	0.52
	2512.2	0.46
	2517.19	0.39
	2522.19	0.33
	2527.18	0.26
	2532.18	0.2
	2537.17	0.13
	2542.17	0.07
	2547.16	0

Appendix C				
Distances and elevations along seismic Line 3				
Measurements are relative to the first shotpoint				
Shot Number	Shot Dist. (m)	Shot Elev. (m)	Geophone Dist.	Geophone Elev. (m)
1	0	1.9	0	1.9
2	5	1.7	5	1.7
3	10	1.5	10	1.5
4	15	1.3	15	1.3
5	20	1.1	20	1.1
6	25	1	25	1
7	30	0.9	30	0.9
8	35	0.8	35	0.8
9	40	0.7	40	0.7
10	45	0.6	45	0.6
11	50	0.5	50	0.5
12	55	0.5	55	0.5
13	60	0.5	60	0.5
14	65	0.5	65	0.5
15	70	0.5	70	0.5
16	75	0.5	75	0.5
17	80	0.5	80	0.5
18	85	0.5	85	0.5
19	90	0.51	90	0.51
20	95	0.53	95	0.53
21	100	0.55	100	0.55
22	105	0.57	105	0.57
23	110	0.59	110	0.59
24	115	0.61	115	0.61
25	120	0.63	120	0.63
26	125	0.65	125	0.65
27	130	0.67	130	0.67
28	135	0.69	135	0.69
29	140	0.71	140.04	0.6
30	144.97	0.73	145.02	0.53
31	149.93	0.75	150.18	0.86
32	154.9	0.77	155.09	0.94
33	160.03	0.88	159.99	1.01
34	165.1	1.05	165.11	1.34
35	170.12	1.52	170.09	1.43
36	175.09	1.61	175.08	1.52
37	180.06	1.71	180.06	1.6
38	185.03	1.8	185.05	1.69
39	190	1.9	190.03	1.78
40	194.97	1.99	195.02	1.87
41	199.94	2.09	200	1.95
42	204.91	2.18	204.99	2.04
43	209.85	2.09	209.97	2.13
44	214.78	2.02	214.96	2.22

45	219.72	1.96	219.94	2.31
46	224.61	2.38	224.93	2.39
47	229.5	2.5	229.91	2.48
48	234.52	2.56	234.9	2.57
49	239.54	2.62	239.88	2.66
50	244.56	2.69	244.87	2.74
51	249.58	2.75	249.85	2.83
52	254.6	2.81	254.84	2.92
53	259.77	2.94	259.82	3.01
54	264.78	2.96	264.81	3.1
55	269.77	3.02	269.79	3.18
56	274.77	3.07	274.78	3.27
57	279.76	3.13	279.76	3.36
58	284.75	3.19	284.75	3.45
59	289.74	3.25	289.73	3.53
60	294.74	3.3	294.72	3.62
61	299.73	3.36	299.7	3.71
62	304.71	3.27	304.73	3.53
63	309.7	3.19	309.69	3.45
64	314.63	2.92	314.67	3.16
65	319.71	3.28	319.7	3.38
66	324.62	3.08	324.66	3.2
67	329.61	2.98	329.62	3.05
68	334.6	2.84	334.62	2.95
69	339.63	2.69	339.57	2.82
70	344.62	2.49	344.52	2.63
71	349.51	2.5	349.33	2.53
72	354.5	2.44	354.37	2.5
73	359.51	2.42	359.36	2.52
74	364.52	2.39	364.35	2.53
75	369.5	2.27	369.35	2.55
76	374.5	2.28	374.34	2.57
77	379.5	2.35	379.33	2.58
78	384.36	2.65	384.32	2.6
79	389.56	2.41	389.42	2.4
80	394.41	1.98	394.47	2.17
81	399.49	2.02	399.32	2.08
82	404.3	2.12	404.42	1.95
83	409.48	1.83	409.32	1.85
84	414.46	1.69	414.3	1.8
85	419.42	1.64	419.28	1.87
86	424.34	1.67	424.11	1.78
87	429.34	1.62	429.22	1.7
88	434.29	1.7	434.33	1.63
89	439.32	1.57	439.25	1.53
90	444.24	1.54	444.22	1.52
91	449.27	1.6	449.14	1.57
92	454.27	1.62	454.06	1.6
93	459.21	1.58	459.19	1.55

94	464.23	1.48	464.11	1.46
95	469.25	1.58	469.02	1.52
96	474.23	1.56	474.11	1.58
97	479.34	1.6	479.03	1.31
98	484.13	1.6	484.03	1.44
99	489.11	1.53	488.95	1.48
100	494.02	1.58	494.01	1.51
101	498.94	1.52	498.91	1.45
102	503.83	1.48	503.76	1.42
103	508.77	1.46	508.92	1.46
104	513.67	1.44	513.88	1.35
105	518.67	1.4	518.83	1.35
106	523.68	1.45	523.51	1.29
107	528.6	1.41	528.44	1.31
108	533.61	1.36	533.46	1.34
109	538.59	1.42	538.44	1.4
110	543.67	1.33	543.78	1.32
111	548.75	1.4	548.74	1.34
112	553.58	1.41	553.72	1.41
113	558.52	1.26	558.64	1.38
114	563.5	1.36	563.59	1.37
115	568.51	1.38	568.53	1.35
116	573.67	1.38	573.56	1.34
117	578.61	1.38	578.56	1.34
118	583.45	1.4	583.48	1.27
119	588.44	1.38	588.67	1.37
120	593.63	1.29	593.58	1.24
121	598.53	1.27	598.53	1.2
122	603.42	1.22	603.48	1.16
123	608.35	1.08	608.32	1.05
124	613.12	0.86	613.14	0.94
125	618.2	1.02	617.98	1.01
126	623.11	0.88	622.9	0.98
127	627.98	0.79	628.02	0.93
128	632.87	0.82	632.68	0.84
129	637.7	0.62	637.72	0.66
130	642.84	0.85	642.79	0.9
131	647.9	0.79	647.63	0.95
132	652.91	0.86	652.67	0.91
133	657.99	0.78	657.78	0.85
134	662.94	0.47	662.76	0.76
135	667.91	0.48	667.73	0.56
136	672.73	0.32	672.45	0.52
137	677.66	0.43	677.5	0.53
138	682.57	0.41	682.57	0.52
139	687.48	0.3	687.59	0.48
140	692.7	0.33	692.69	0.37
141	697.72	0.37	697.87	0.35
142	702.57	0.17	702.69	0.29

143	707.6	0.24	707.65	0.22
144	712.62	0.24	712.79	0.22
145	717.68	0.2	717.77	0.16
146	722.69	0.08	722.53	0.13
147	727.77	0.2	727.55	0.19
148	732.93	0.16	732.53	0.29
149	737.62	0.18	737.53	0.15
150	742.74	0.13	742.57	0.11
151	747.77	0.03	747.71	0.04
152	752.83	0	752.74	-0.02
153	757.48	0.05	757.47	0.05
154	762.39	0.05	762.32	0.13
155	767.16	0.24	767.35	0.27
156	772.45	0.23	772.45	0.35
157	777.32	0.23	777.41	0.35
158	782.37	0.29	782.36	0.38
159	787.63	0.38	787.29	0.43
160	792.53	0.41	792.39	0.42
161	797.4	0.47	797.14	0.49
162	802.35	0.55	802.19	0.58
163	807.22	0.5	807.43	0.62
164	812.12	0.56	812.3	0.66
165	817.07	0.64	817.15	0.69
166	822.01	0.67	822.16	0.75
167	827.12	0.71	826.98	0.8
168	832.01	0.76	831.94	0.8
170	842.16	0.91	837.2	0.85
171	847.05	0.99	841.92	0.97
172	852.05	0.97	847.08	1.01
173	857	0.93	852.17	0.95
174	861.74	0.94	856.89	0.99
175	867.01	0.96	861.96	0.95
176	871.89	1.02	867.02	0.96
177	877.02	1.03	871.91	1.05
178	881.82	0.94	876.95	0.97
179	886.86	1.08	881.86	0.98
180	891.9	1.2		
182	901.72	1.32		
187	926.65	0.46		

Elev(m)
30
20
10
0

Appendix D (i)

Line 2

0
300
600
90

Depth (m)
0
100
200
300
400
500

Appendix D (ii)

Line 2

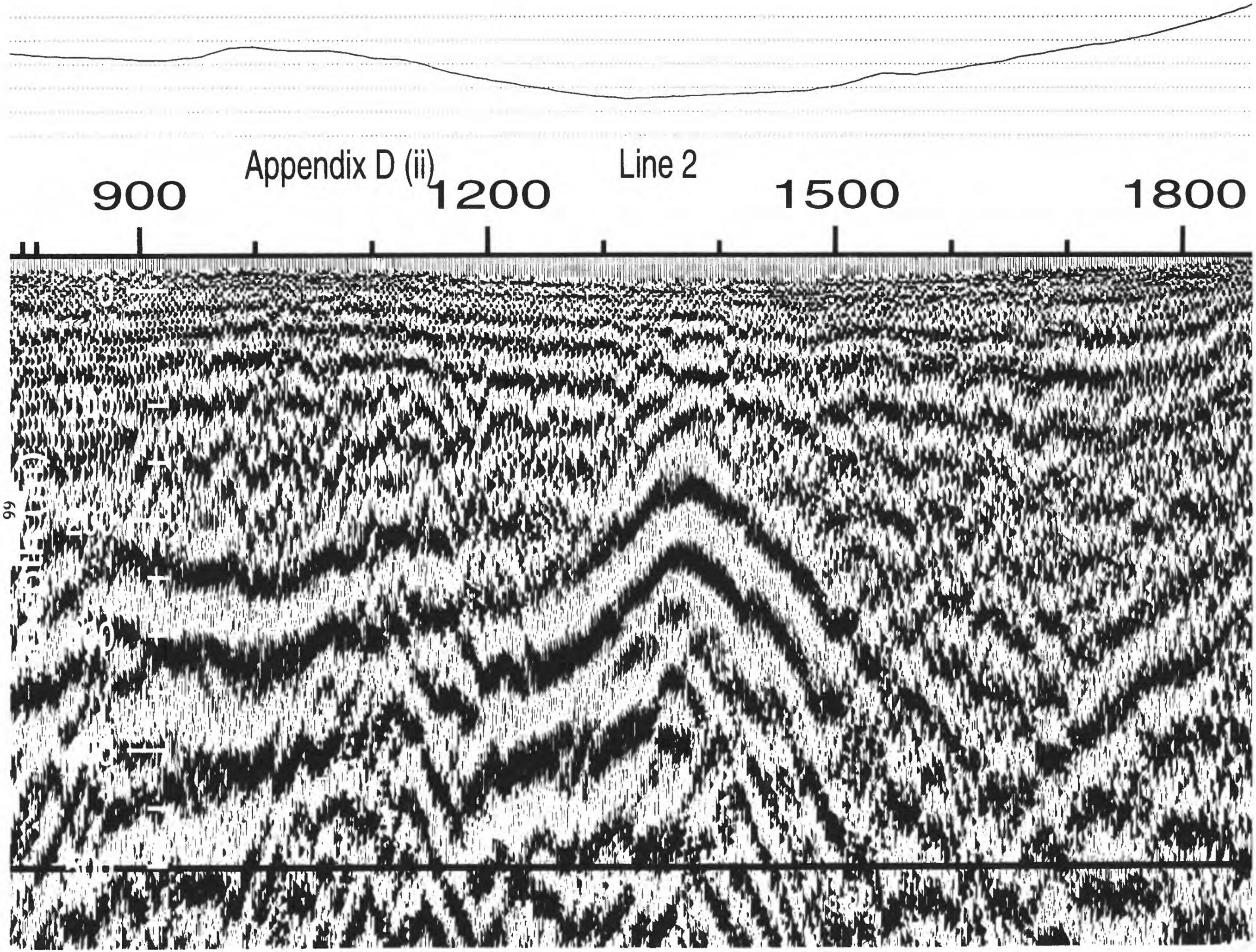

Appendix D (iii)

Line 2

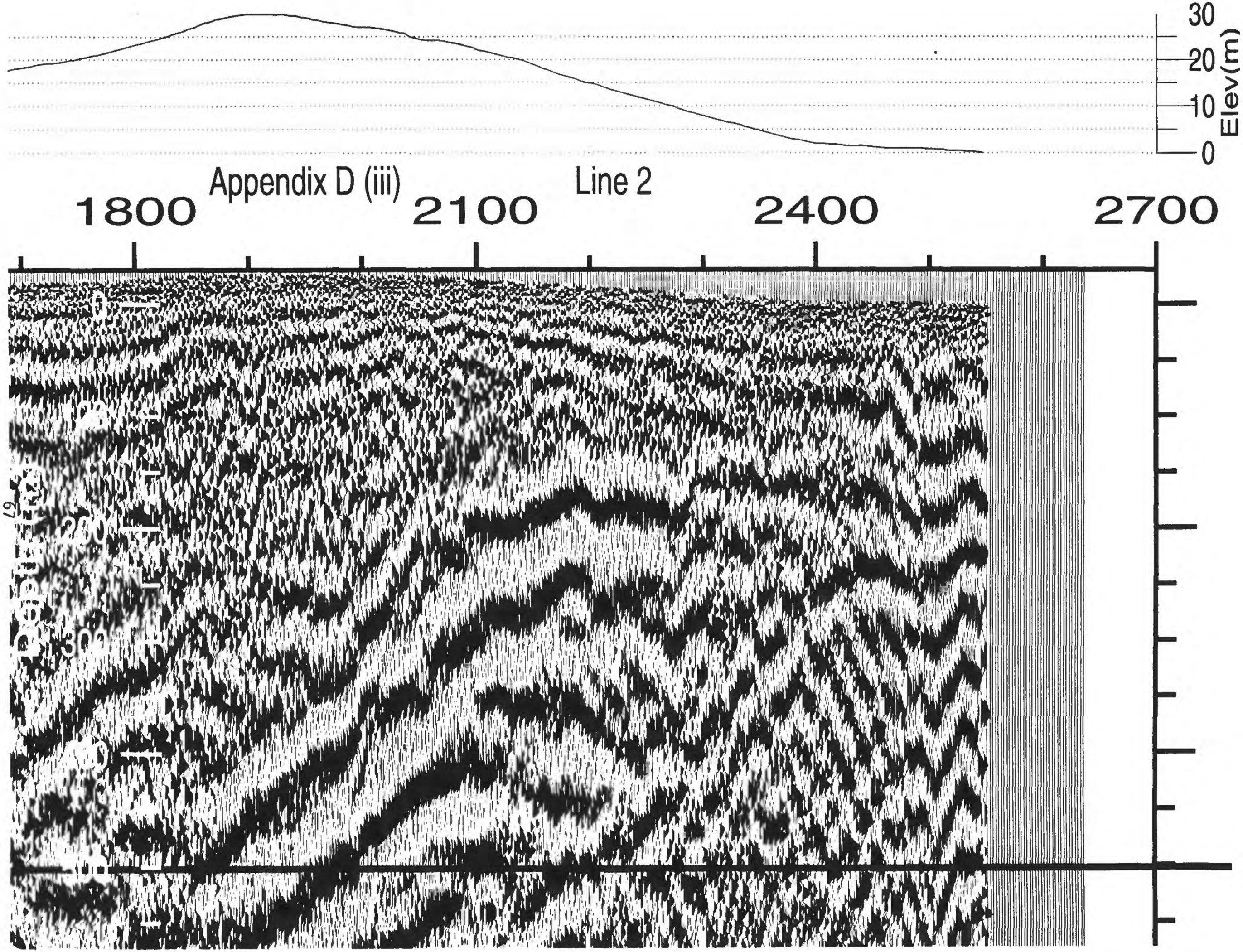

Appendix E (i)

Line 3

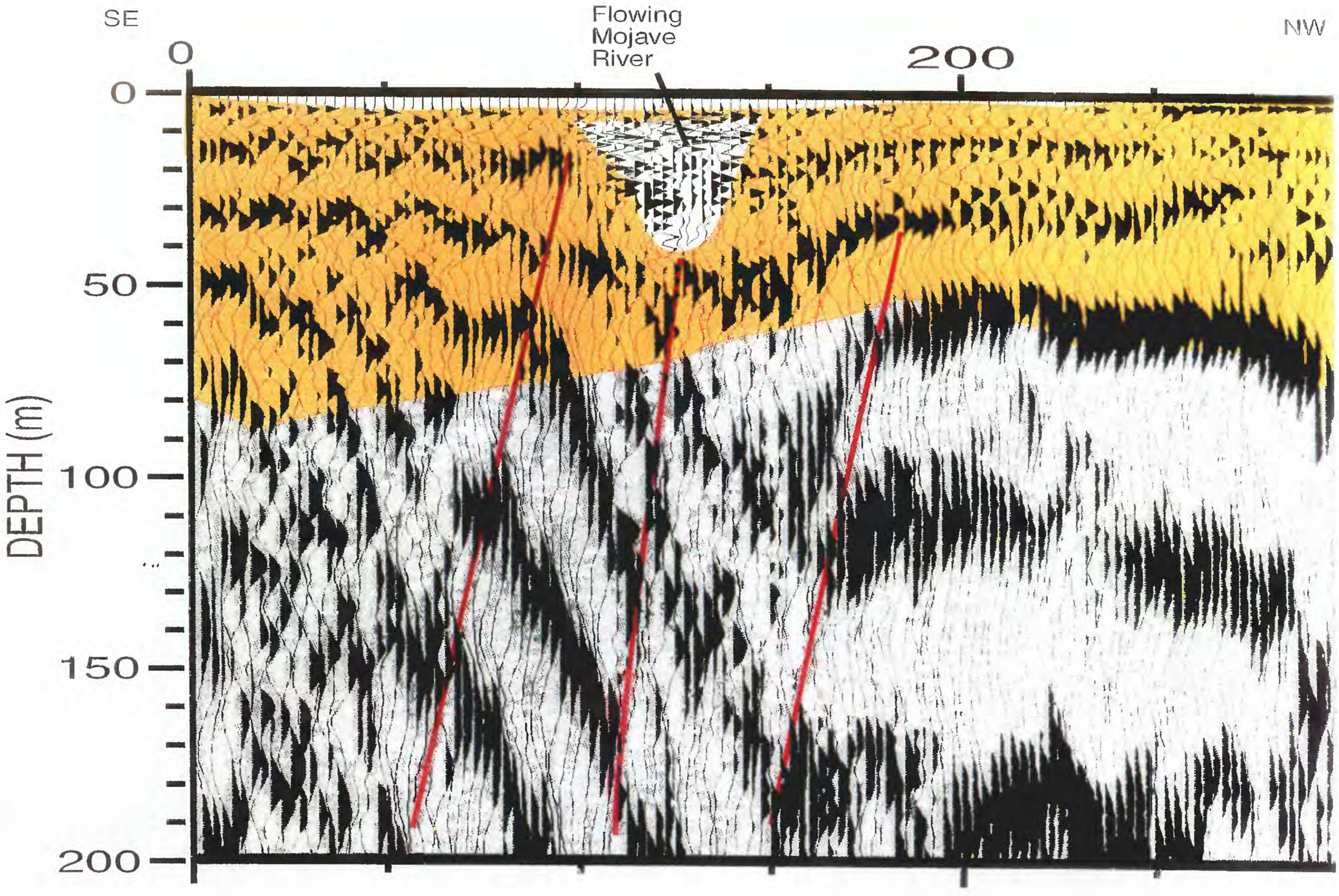

Appendix E (i)

Line 3

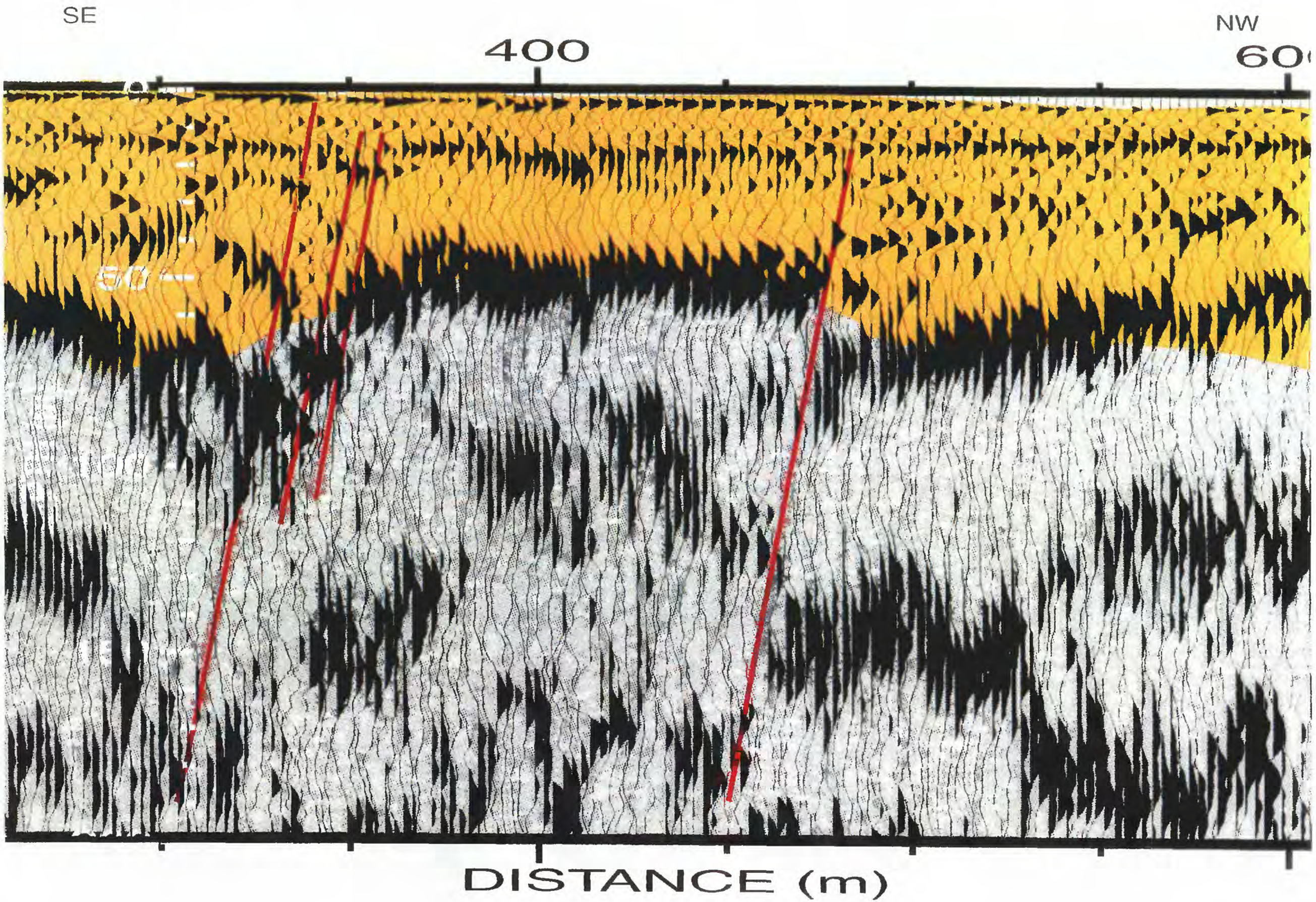

Appendix E (ii)

Line 3